High-resolution single cell transcriptome analysis of zebrafish sensory hair cell regeneration

Sungmin Baek[1], Nhung T. T. Tran[1], Daniel C. Diaz[1,2], Ya-Yin Tsai[1] and Tatjana Piotrowski[1,3#]

[1]Stowers Institute for Medical Research, 1000 East 50th Street, Kansas City, MO 64110
[2]Current address: Parse Biosciences, 201 Elliott Ave W, Suite 290 Seattle, WA 98119
[3]Lead Contact

#Correspondence: pio@stowers.org

Key words: hair cell regeneration, scRNA-Seq atlas, lateral line, support cells, stem cells

Summary

Loss of sensory hair cells in the mammalian inner ear leads to permanent hearing and vestibular defects, whereas loss of hair cells in zebrafish results in their regeneration. We used scRNA-Seq to characterize the transcriptional dynamics of hair cell regeneration in zebrafish at unprecedented spatio-temporal resolution. We uncovered three, sequentially activated modules. First, an injury/inflammatory response and downregulation of progenitor/stem cell maintenance genes within minutes after hair cell loss. Second, the transient activation of regeneration-specific genes. And third, a robust reactivation of developmental gene programs, including hair cell specification, cell cycle activation, ribosome biogenesis, and a metabolic switch to oxidative phosphorylation. The results are not only relevant for our understanding of hair cell regeneration and how we might be able to trigger it in mammals but also for regenerative processes in general. The data is searchable and publicly accessible via a web-based interface.

Introduction

Humans in particular, and mammals in general, fail to regenerate mechanosensory hair cells in their inner ears. Noise, drug or age-induced hearing loss due to hair cell death is, therefore, permanent (Furness, 2015; Wagner and Shin, 2019; Wong and Ryan, 2015). In contrast, fish, chicken and amphibians constantly replace dying hair cells through proliferation and differentiation of support cells (Corwin and Cotanche, 1988; Corwin and Warchol, 1991; Cruz et al., 2015; Pinto-Teixeira et al., 2015; Ryals and Rubel, 1988). Because neonatal mouse support cells are able to produce a modest number of hair cells after injury and some vestibular hair cells turn over spontaneously, there is hope that elucidating the gene regulatory networks underpinning hair cell regeneration, may lead to the restoration of hearing loss. (Bucks et al., 2017; Burns et al., 2012; Burns and Stone, 2017; Cox et al., 2014; Du et al., 2013; Forge et al., 1993; Korrapati et al., 2013; Warchol and Corwin, 1996; White et al., 2006). One strategy to identify candidate genes and pathways that might trigger hair cell regeneration in mammals has been to identify genes involved in hair cell

development (Burns et al., 2015; Cai and Groves, 2015; Jen et al., 2019; Lee et al., 2020; Sayyid et al., 2019; Scheffer et al., 2015; Valdivia et al., 2011; Zhu et al., 2019). Another promising strategy is to identify the molecular underpinnings of hair cell regeneration in regenerating species, such as chicken and zebrafish and use this blueprint of regeneration to experimentally trigger regeneration in mammals (Behra et al., 2009; Jiang et al., 2014; Ku et al., 2014; Pei et al., 2018; Roccio et al., 2018; Scheibinger et al., 2018; Steiner et al., 2014). However, the number of regenerated hair cells and hearing improvement attained in mammals thus far has been modest. This is likely due to the limited number of known candidate genes and our general lack of understanding of hair cell type specific expression dynamics at a fine time scale.

The zebrafish sensory lateral line is a powerful model to study hair cell development and regeneration because of its accessibility and relative ease of experimental manipulation (Figure 1A; (Denans et al., 2019; Kniss et al., 2016; Lush and Piotrowski, 2014; Ma and Raible, 2009; Romero-Carvajal et al., 2015; Viader-Llargues et al., 2018)). Zebrafish and mammalian sensory hair cells are very similar, and loss of lateral line hair cell genes does not only cause loss of hair cell function in fish, but also causes deafness and vestibular dysfunction in mammals (Nicolson, 2005; Whitfield, 2002).

We have previously performed bulk RNA-Seq analyses of regenerating lateral line hair cells that identified candidate genes and pathways. However, this study lacked spatio-temporal resolution (Jiang et al., 2014). To identify the cell populations involved in regeneration, we analyzed the different cell populations that respond to hair cell death in time lapse and BrdU analyses and have characterized all cell populations in homeostatic lateral line sensory organs (neuromasts) using scRNA-Seq (Figures 1B-E; (Lush et al., 2019; Romero-Carvajal et al., 2015)). Lateral line sensory organs consist of sensory hair cells surrounded by support cells and an outermost ring of mantle cells. Support cells can be subdivided into anterior-posterior (A/P), dorso-ventral (D/V) and a central sub population (Romero-Carvajal et al., 2015; Thomas and Raible, 2019; Wibowo et al., 2011). During regeneration support cells divide before differentiating into hair cells (López-Schier and Hudspeth, 2006; Ma et al., 2008; Mackenzie and Raible,

2012; Wibowo et al., 2011). Central support cells are the immediate precursors of hair cells (Lush et al., 2019; Romero-Carvajal et al., 2015). D/V and A/P support cells also give rise to hair cells but it is not known if they first acquire a central support cell fate or if they directly differentiate into hair cells during regeneration. Mantle cells do not respond behaviorally to hair cell loss, but they generate support cells and hair cells after severe injury to the sensory organ (Denans et al., 2019; Romero-Carvajal et al., 2015; Thomas and Raible, 2019; Viader-Llargues et al., 2018).

Previous studies have shown that all regenerative cell divisions are symmetric. Central and A/P support cells divide and give rise to two hair cells, whereas D/V cells that are in contact with mantle cells (amplifying cells) also divide symmetrically but do not differentiate and instead give rise to two support cells (Romero-Carvajal et al., 2015). Manipulations of the Notch and Wnt signaling pathways demonstrated that the majority, or maybe even all support cell populations can be induced to proliferate and either give rise to only hair cells or to only support cells. We therefore concluded that the majority of support cells are competent to serve as hair cell progenitors.

Faithful regeneration of sensory cells requires the precise orchestration of stem/progenitor cell activation, proliferation, cell lineage determination and differentiation. Of all the vertebrate regeneration models studied, such as fin, heart and retina regeneration, hair cell regeneration is by far the fastest. Zebrafish lateral line cells die within 30min of killing hair cells and the first newly regenerated hair cells arise around 5 hours later. Differential gene expression, enrichment term analysis, pseudotime analysis, and validation by in situ hybridization allowed us to define the molecular changes taking place during hair cell regeneration at unprecedented levels of resolution. We correlated the transcriptional dynamics with previously defined cellular behaviors to build the foundation for the establishment of a gene regulatory network (GRN). We discovered three, sequentially activated modules. The first module consists of a systemic injury/inflammatory response, which likely plays a crucial role in the initiation of regeneration (Beisaw et al., 2020; Wang et al., 2020). The second module is characterized by a transient activation of regeneration-specific genes. The longest, third phase of regeneration recapitulates developmental events. Thus, once

121 initiated, regeneration recapitulates development but the early injury/inflammatory
122 response is regeneration-specific. The resulting gene expression dynamics are publicly
123 available and readily searchable via web-based interfaces:
124 https://piotrowskilab.shinyapps.io/neuromast_regeneration_scRNA-Seq_pub_2021/
125 and gEAR (https://umgear.org/p?l=e0d00950) (Orvis et al., 2021).
126 Knowing when and in which cell types genes and pathways are modulated, and
127 when lineage decisions occur informs not only our understanding of zebrafish lateral
128 line hair cell regenerate but also efforts to induce hair cell regeneration in mammals.
129 Therefore, the high spatio-temporal resolution data presented here can serve to
130 determine whether different injury paradigms lead to different transcriptional responses
131 and provide a foundation for comparative regeneration studies across species and
132 different regenerating organs.
133
134 **Results**
135 To determine the stages for transcriptomic analyses, we analyzed time lapse
136 recordings of regenerating hair cells (Figure 1F). The vast majority of hair cells are dead
137 within 30min of addition of neomycin, and dead hair cell debris is cleared between 3-
138 5h hours. Hair cells regenerate rapidly, with the first new pair detected within 3- 5
139 hours after neomycin exposure (Figure 1F, arrow; (Romero-Carvajal et al., 2015)). To
140 characterize the transcriptional changes that underly these fast behavioral responses,
141 we performed single cell RNA-Seq (scRNA-Seq) using the 10X Chromium platform
142 during homeostasis (homeo) and six time points after 30 min neomycin exposure to kill
143 hair cells (Figure 1F, homeo, 0 min, 30 min, 1h, 3h, 5h and 10h). We dissociated 5dpf
144 *Tg(she:H2A-mCherry)* fish, in which all neuromast cells are labeled (Peloggia et al.,
145 2021). After sequencing, we integrated cells from all time points using Seurat (v3.2.0)
146 and plotted them in two-dimensional UMAP space (Figure 1G). Cluster analyses
147 identified the same populations we previously described in homeostatic neuromasts
148 (Figure 1H, Figures 1B-E; (Lush and Piotrowski, 2014)). Figure 1I and Figure S1A show
149 the expression of selected cluster marker genes in UMAP space (Table S1). We did not

150 observe any obvious loss or gain of a particular population during any of the
151 regeneration time points (Figures S1B-C).
152 We show the results of the transcriptome analyses of all 6 time points after hair cell
153 death using all cells in Figure 1- Figure 5, and present the results of pseudotime
154 analyses using only central support cells and cells belonging to the hair cell lineage in
155 Figure 6 – Figure 8. The results of our regeneration analysis can be queried using
156 publicly available databases: the shiny app entitled 'Neuromast Regeneration scRNA-
157 Seq' shows feature plots, violin plots, dot plots and heat maps of the entire data set,
158 whereas the link within this shiny app called 'Pseudotime Analysis' shows feature
159 plots, violin plots, dot plots and line graphs of central cells and hair cell lineage (Figures
160 S2A-B, https://piotrowskilab.shinyapps.io/neuromast_regeneration_scRNA-
161 Seq_pub_2021/). The genes present in both databases are listed in table S2. In
162 addition, the data has been deposited to gEAR, a database that allows comparison of
163 our data with other published data from other species (Figure S2C,
164 https://umgear.org/p?l=e0d00950)(Orvis et al., 2021).
165 The transcriptional responses to hair cell death are rapid and cohorts of genes
166 are robustly down and up-regulated immediately after hair cell death (0min time point,
167 Figure 1J). These fast transcriptional changes continue throughout regeneration.
168 UMAPs of individual cell types, in which cells are grouped according to the degree of
169 similarity in their transcriptomes, show that cells at the 0min time point have a
170 drastically different transcriptome than homeostatic cells and the 30min time point
171 (Figures 1K-N). Cells collected at the 30min and 1h time points are more similar to
172 each other but distinct from the 3h-10h time points. 5 and 10h cells are
173 transcriptionally most similar to homeostatic cells. These groupings are not caused by
174 batch effects as cells collected at different time points possess similar number of UMI
175 count distribution (Figure S1D). The largest number of transcriptional changes occur in
176 central, A/P, D/V and hair cell progenitor cells, whereas amplifying cells, hair cell
177 progenitors, young and mature hair cells show a much smaller response (Figures 1K-N,
178 Figures S1E-G). Mantle cells also show robust transcriptional changes, even though
179 they do not proliferate in response to neomycin-induced hair cell death (Figure S1H;

180 (Romero-Carvajal et al., 2015)). We observed the largest number of upregulated
181 transcripts at 3h after hair cell death, whereas between 0min- 1h more genes are
182 down- than upregulated.
183 In summary, our transcriptome analysis of closely spaced time points revealed
184 that transcriptome changes occur rapidly in support cell populations immediately after
185 killing hair cells. The different regeneration time points can be roughly grouped into
186 three modules: 0min, 30min/1h and 3h/5h/10h. 10h cells begin to resemble
187 homeostatic cells. To determine what transcriptional changes occur between the three
188 modules we performed differential gene expression between various combinations of
189 time points and selected genes that changed in several cell types or specifically in
190 some cell populations (Table S3 (differentially expressed genes) and Table S4 (plotted
191 genes shown in Figures).
192
193 **Module 1 (0min): Modulation of progenitor/stem cell maintenance/placodal and**
194 **injury/inflammatory response genes**
195 Progenitor/stem cell maintenance/placodal genes are rapidly turned off after
196 neomycin treatment but are re-expressed between 3- 5h (Figure 2, Figure S3, Table
197 S4). In contrast, injury/inflammatory genes are rapidly activated after hair cell death but
198 are also sharply turned off again after 30min- 1h (Figure 3, Figure S4, Table S4).
199
200 *Downregulation of progenitor/stem cell maintenance/placodal genes, Notch- and Fgf*
201 *signaling 0min after hair cell death*
202 0min after neomycin treatment, we observed that more genes are
203 downregulated than upregulated (Figures 1K-N). A heatmap of the downregulated
204 genes in different cell types and at different time points shows that the downregulation
205 of genes at 0min is transient and that the majority of genes are re-expressed between
206 3-10h (Figure 2A, Table S4). It is also apparent that many downregulated genes are cell
207 type specific. Among the downregulated genes are several involved in ear/lateral line
208 placode development, including stem cell markers, such as *sox2/3*, as well as the
209 Notch-, and Fgf signaling pathways (Figures 2B-E, Table S4; (Graham et al., 2003;

210 Hernandez et al., 2007; Jiang et al., 2014; Sarkar and Hochedlinger, 2013)). We
211 validated the downregulation of these genes by in situ analysis (Figure 2C, also (Jiang
212 et al., 2014)). To test whether the observed downregulation is not caused by the
213 neomycin treatment, we treated *atoh1a* mutant larvae, which lack hair cells with
214 neomycin (Figure 2C). *sox2* is only downregulated after hair cell death in the siblings at
215 0min demonstrating that the downregulation of genes is not caused by the neomycin
216 treatment but by the loss of hair cells. Figure S3A shows in which cell types different
217 placodal genes are enriched. Prior studies showed that Notch and Fgf signaling are
218 downregulated to allow for Wnt-dependent cell proliferation (Lush et al., 2019;
219 Romero-Carvajal et al., 2015). Notch downregulation is also required to initiate hair cell
220 differentiation (Ma et al., 2008; Romero-Carvajal et al., 2015; Wibowo et al., 2011).
221 *vegfab* is also downregulated at 0 min but re-expressed by 10h (Figure 2A central
222 cells). Interestingly, Vegf is required for hair cell regeneration in the avian ear (Wan et
223 al., 2020), but a role for Vegf signaling in the lateral line has not been previously
224 described.
225 Enrichment term analyses show that the most drastically downregulated
226 processes are oxidative phosphorylation (OXPHOS), ribosomal proteins, genes
227 involved in splicing and the Notch pathway (Figure 2F, Figure S3B, Table S3). These
228 terms suggest that translation is inhibited and that the lateral line progenitor/stem cells
229 undergo metabolic reprogramming from OXPHOS to glycolysis, a characteristic of
230 other stem cells that become activated (Mathieu and Ruohola-Baker, 2017; Shyh-
231 Chang and Ng, 2017).
232
233 *Upregulation of the injury/inflammatory response at 0min: AP-1 complex, Tnf-, IFNg,*
234 *Tgfb and glucocorticoid signaling*
235 Injury either induces early response genes in all support cell types (Figures 3A-
236 B) or only central-, A/P-, amp-, or mantle cells (Figures 3C-F, Table S4; (Bahrami and
237 Drablos, 2016)). Some early response genes are known to be involved in an
238 inflammatory response that, depending on the context and timing have either pro- or
239 anti-regenerative effects (Eming et al., 2017; Kyritsis et al., 2012; Namdaran et al.,

240 2012; White et al., 2017). We found that AP-1 complex members (eg., *fosab, fosb,*
241 *fosl1a, jund, junba*), the nuclear hormone receptor *nr4a1* and other early response
242 genes, such as *atf3*, *egr1*, and *btg2* are strikingly upregulated at 0min but are turned off
243 again at 30min (Figures 3A, G, H, M, Figure S4A; (Cho et al., 2004)). Because AP-1
244 family members and *nr4a1* respond to injury/inflammation, we wondered whether the
245 neomycin treatment, rather than hair cell death causes the upregulation of these genes.
246 We treated sibling and *atoh1a* mutants that do not possess hair cells with neomycin
247 and performed in situ hybridization with *fosab* and *nr4a1* (Figures 3I-J). *atoh1a* mutant
248 neuromasts do not upregulate these genes in response to neomycin treatment
249 demonstrating that they are specifically upregulated in response to hair cell death. We
250 then tested whether *nr4a1* upregulation is induced by hair cell death specifically
251 (Figures 3K-L). We laser-ablated support cells in siblings and *atoh1a* mutants and
252 found *nr4a1* expression induced in both, demonstrating that death of any cell type
253 leads to the upregulation of injury response genes.
254 Glucocorticoid and Jak/Stat signaling, as well as *immunoresponsive gene 1-like*
255 (*irg1l)* are also activated in most cell types at 0min, but Jak/Stat and *irg1l* stay on until
256 30min/1h (Figure 3N, Figures S4A-B, D). *irg1l* is induced in keratinocytes by
257 macrophages after infection and in turn leads to metabolic reprogramming in
258 macrophages (Hall et al., 2014). Its role in lateral line regeneration needs to be
259 determined. Interferon-, and Tgfβ signaling are activated slightly later than the early
260 response genes and are expressed in distinct subset of cell types (Figure 3O, Figures
261 S4C, D). Other genes are specifically enriched in particular cell types at 0min-1h, such
262 as *egr2b*, *ch25h* and *hbegfb* in central cells and the autophagy gene *map1lc3cl* in AP
263 cells (Figure 3A, Figures S4A, D). Why these genes are activated in some but not all cell
264 types remains to be investigated. Other enrichment terms describing genes
265 upregulated at 0min are MAPK signaling, Toll-like receptor signaling and cell adhesion
266 molecules (Figure 3P, Figure S3B, Table S3).
267
268
269

Module 2 (30min -1h): Regeneration-enriched genes are upregulated

30min- 1h genes are only lowly expressed in homeostatic sensory organs but are robustly induced for a short period during regeneration (Figure 4, Figure S5)

Regeneration specific genes, translation, RA-, MAPK signaling and cell adhesion are induced between 30min- 1h

Module 2 genes are either upregulated in all support cells and hair cell progenitors at 30 min (Figures 4A, F, H, I, K, Table S4) or they are specifically upregulated in young and mature hair cells (*lin28a*, *irx2a* and *pak1*; Figures 4B, I); some central support cells and the hair cell lineage (*gadd45ga*, *sox4a1*, *kitlga*; Figure 4B); the central support cells (e.g. *cd44a*, *crabp2a*, *il11b*, *noxa1*, *rln3a*, *tgfb1a*, *arid3a*; Figures 4C, G); AP cells (Figure 4D) and mantle cells (Figure 4E). Retinoic acid (RA) signaling is also induced between 30min and 1h with pathway members being expressed in different cell types (Figures 4J-K, Figure S5). Enrichment terms that characterize upregulated genes at 30min are the MAPK cascade, NOD-like receptor signaling and Cell adhesion/tight junction, whereas ectodermal placode/otic vesicle development, Notch signaling, TCF-dependent Wnt signaling and oxidative phosphorylation are downregulated (Figure 4L, Figure S3B, Table S3). At 1h, ribosomal and other translation-associated genes are induced, whereas signaling by Wnt, Notch, cell differentiation and metabolism is still downregulated (Figure 4L, Figure S3B, Table S3).

Module 3 (3h- 10h): Recapitulation of hair cell development

Genes expressed between 3h- 10h are expressed during development, as well as during hair cell turnover during homeostasis (Figure 5, Figure S6 and S7 (Romero-Carvajal et al., 2015)).

At 3h the hair cell lineage becomes specified and ribosome biogenesis and splicing gene expression is activated

At 3h a few genes are upregulated in all cell types, such as *apoa2*, *ccl34b.1*, *lmo4b* and *nkx3.2* (Figure 5A, Table S4); however, the majority of 3h genes detected by

300 3h show cell-type specific expression (Figures 5B-E). Ribosome biogenesis genes and
301 splicing factor expression particularly increase in HC progenitors, whereas epigenetic
302 regulators are most highly expressed in young hair cells (Figures 5F, G, H, Figure S6A-
303 B, Table S4). Figure S7 shows the heatmap of all genes shown in the dot plots, as not
304 all are represented in Figures 5A-E. As a measure of the robustness of our scRNA-Seq,
305 we generated dot plots and heat maps of ribosome biogenesis GO term genes and
306 spliceosome pathway members listed in KEGG (Table S3). Indeed, these genes are
307 highly enriched at 3-5h (Figures S6A-B). Thus, even genes that were not
308 identified/filtered out in our differential gene expression analysis are expressed in our
309 data set and can be queried using the shiny app or gEAR (Figure S2)(Orvis et al., 2021).
310 Also, the hair cell specifying gene *atoh1a* is upregulated in hair cell progenitors
311 and young hair cells at 3h (Bermingham et al., 1999; Chen et al., 2002; Gubbels et al.,
312 2008; Woods et al., 2004; Zheng and Gao, 2000), and downstream hair cell lineage
313 targets, such as *delta* ligands, *myclb*, *gadd45gb*.1 and *kdm6bb* are upregulated by 5h
314 (Figures 5C, I, Table S4). The percentage of hair cell progenitors and young hair cells
315 that express these genes is shown in Figure S6C. In the heatmap Figures 5A-E, we
316 omitted cell cycle genes. Figure 5J shows that cell cycle genes are also enriched at 3h
317 and are most highly expressed in amplifying cells (Figure 5M, Table S4). Amplifying
318 cells are located in the poles of the sensory organs and proliferate to give rise to more
319 support cells (Figure 1D). They do not differentiate into hair cells unless they are
320 displaced into the center of the sensory organ (Romero-Carvajal et al., 2015). Cell cycle
321 genes are also activated in hair cell progenitors and young hair cells at 3h (Figures 5J,
322 M). Early cell cycle genes involved in DNA replication, such as *mcm* genes, are
323 enriched in hair cell progenitors and AP cells, whereas young hair cells and DV cells
324 express genes characteristic of later stages of the cell cycle (Figure 5M). Thus, the hair
325 cell lineage is tightly associated with proliferation in lateral line regeneration. Wnt
326 signaling regulates proliferation in the lateral line (Jacques et al., 2013; Romero-
327 Carvajal et al., 2015) and our data indicate that this pathway is reactivated at 3h (Figure
328 5K). We also find that Wnt pathway genes are enriched in the different support cell
329 populations but are downregulated in hair cell progenitors and hair cells (Figure S6D).

330 Most notably, Notch pathway genes are re-expressed by 5h, as well as genes
331 associated with oxidative phosphorylation (Figure 5L, Figures S6G-H) (Liberzon et al.,
332 2015). Figures S6E-F show an expanded list of Notch pathway genes and the cell
333 types in which they are enriched. We observe that ribosome biogenesis and splicing
334 commence by 3h, whereas oxidative phosphorylation and the Notch/Wnt signaling
335 pathways are reactivated by 5h (Figures 5N-P, Figure S3B, Table S3). Furthermore,
336 focal adhesion, tight junction and cell adhesion genes are downregulated during these
337 time points, a hallmark of proliferating epithelial cell. In fact, many of the genes
338 associated with otic vesicle/ectodermal placode development such as *sox2* and *sox3*
339 are re-expressed by 10h, while MAPK signaling and translation genes are markedly
340 downregulated. Altogether, our data indicate that the discrete waves of gene up and
341 downregulation observed during hair cell regeneration closely recapitulate key aspects
342 of hair cell development.
343
344 **Pseudotime analysis indicates that central support cells either differentiate into**
345 **hair cells or they re-express support cell genes**
346 To gain a better understanding of the lineage trajectories that central support
347 cells (central SCs) undergo during regeneration and to identify associated genes, we
348 aligned central support-, progenitor- and hair cells along pseudotime using Monocle 3
349 (Cui et al., 2020; Qiu et al., 2017; Trapnell et al., 2014). We chose to limit the analysis to
350 these cell types, as in vivo lineage tracing showed that central support cells are the
351 direct precursors to hair cells (Lush et al., 2019). Although D/V and A/P cells can also
352 give rise to hair cells (Romero-Carvajal et al., 2015; Thomas and Raible, 2019; Wibowo
353 et al., 2011), it still needs to be determined whether A/P and D/V cells first acquire a
354 central support cell fate. Therefore, we focused our analysis on central support cells to
355 analyze hair cell and support cell lineage decisions.
356 To generate the UMAP in Figure 6A we specified 0min central cells (in purple) as
357 the start of the trajectory. Cells with later pseudotime values are colored in yellow. The
358 black line is the fitted trajectory along pseudotime and indicates lineage decisions that
359 cells can take. In contrast to the differential gene expression performed on all cells

360 from all time points (Figure 2- Figure 5), pseudotime analysis reveals a branch point at
361 which cells either follow a path to hair cell differentiation (Figure 6B, lower branch) or
362 they take a trajectory to revert back to a central support cell state (Figure 6B, upper
363 branch). The pseudotime lineage trajectory model is temporally consistent with the
364 regeneration time points that the cells were collected at, with 10h hair cells and 10h
365 central support cells being at the end of each of the two lower and upper branch
366 trajectories, respectively.
367 The branch point at which cells are predicted to undergo a lineage decision
368 occurs in cells at the 3- 5h time points (Figure 6B). To identify the genes that are
369 expressed in cells before the branch point, we aggregated cells into Louvain clusters
370 and performed a differential gene expression analysis between clusters of these
371 different cell groupings/lineages (Figure 6C, Table S5). This analysis showed that sets
372 of genes are progressively activated or de-activated in the injury response and
373 progenitor activation cluster (Figure 6C clusters 3, 2, 7 and 6), the central support cell
374 lineage (Figure 6C clusters 9, 10, and 4), and the hair cell lineage (Figure 6C clusters 8,
375 5, and 1). For instance, the injury response and progenitor activation clusters are
376 characterized by the activation of *cd44a* (Figure 6D), while the central support cell
377 lineage is marked by the upregulation of *gata2b* (Figure 6E). The hair cell lineage cluster
378 is represented by the expression of *rbm24a*, an RNA-binding protein that regulates
379 alternative splicing (Figure 6F).
380
381 *Genes modulated in central support cells before the branch point*
382 The heatmap (Figure 6G) and feature plots show genes that are immediately
383 upregulated in cluster 3 (Figure 6C) central support cells in response to hair cell death
384 but that are off in cluster 2, such as *fosab* (Figures 6 G, H, Figure S8A, Table S5);
385 genes that are upregulated in clusters 3, 2, 7, 6, (Figure 6C) such as *irg1l* (consisting
386 mostly of 30min and 1h central cells, Figures 6G, I, Figure S8A, Table S5); and genes
387 that are most highly expressed in clusters 6 and 7 (Figure 6C) before the branch point,
388 such as *lima1a* (Figures 6G, J, Figure S8A, Table S5). Line graphs of scaled gene

389 expression of *fosab*, *irg1l* and *lima1a* in cells aligned along pseudotime clearly show
390 these distinct gene expression dynamics (Figures 6K, L).
391
392 *Genes modulated in the central support cell lineage after the branch point*
393 To identify genes expressed in the central support cell lineage versus the hair
394 cell lineage after the branch point, we specified the end and start points of each
395 lineage and the algorithm assigned cells at and beyond the branch point to either
396 lineage (Figure S8B). Cells before the branch point are shared between both lineages.
397 The central support cell lineage chiefly consists of clusters 9, 10 and 4 (Figure 6C) and
398 the expression dynamics of genes enriched in these clusters is shown in Figure 7A.
399 Among the genes enriched in the central support cell lineage after the branch point are
400 many of the placodal/stem cell-associated genes, such as *sox2*, *sox3*, *gata2a*, *gata2b*,
401 *klf2a*, *klf17* and *prox1a* (Figure 7B; Figure S9, Table S5). *sox3* is already upregulated
402 before the branch point but then rapidly turned off in the hair cell lineage (Figure 7B).
403 Plotting the expression of these genes in a heatmap that contains all cell types and
404 homeostatic cells shows that many of the central support cell lineage genes are also
405 present during homeostasis. A number of these genes are also expressed in 10h A/P
406 cells and mantle cells suggesting that these cell types also return to their homeostatic
407 transcriptional state (Figure S9).
408 Notably, the Notch pathway is also upregulated (Figure 7C, Figure 5L) along
409 pseudotime and highest in cluster 4 cells (Figures 6B-C, 10h central cells). Line plots of
410 scaled gene expression along pseudotime show that *sox3*, *prox1a* and the Notch
411 target *hey1* are upregulated in the central support cell lineage (Figure 7D).
412 We conclude from these analyses that the central support cells are on a
413 trajectory back to becoming homeostatic central support cells. Indeed, the majority of
414 the central support cell lineage genes are expressed at homeostasis but are
415 subsequently downregulated at 0min, and are later re-expressed between 3-10h
416 (Figure S9).
417
418

419 *Genes modulated in the hair cell lineage*

420 Atoh1 is required for hair cell specification but is not sufficient to regenerate a
421 fully functional sensory epithelium when overexpressed in mammals of in culture
422 (Burns and Stone, 2017; Jen et al., 2019). To identify additional genes that show similar
423 expression dynamics as *atoh1a* or that could be acting upstream of *atoh1a*, we
424 compared gene expression between central support cells and hair cell lineage clusters
425 8, 5 and 1 (Figure 6C, Table S5). Cluster 8 cells are hair cell progenitors and 5 and 1
426 consist of young and mature hair cells, respectively. Differential gene expression
427 analysis between combinations of clusters shows the progression of gene expression
428 along pseudotime (Figure 8A, cell cycle genes were excluded). We were particularly
429 interested in identifying genes that might be involved in specifying hair cells and that
430 act upstream of the hair cell specifier *atoh1a*. *sox4a* (called *sox4a*1* in our data sets) is
431 an attractive candidate, as it is involved in hair cell development (Gnedeva and
432 Hudspeth, 2015) and is expressed in a few central cells, as well as the hair cell lineage
433 (Figure 8B; (Lush et al., 2019)). Indeed, our scRNA-Seq analysis shows that *sox4a* is
434 upregulated before *atoh1a* at 30 min, whereas *atoh1a* is activated at 3h (Figure 5I,
435 Figures 8B, C, Figures S10A-D). Both genes are expressed in central cells and the hair
436 cell lineage (Figures S10C, D). We validated this difference in the onset of gene
437 expression after hair cell death using HCR in situ hybridization (Figures 8E, F). Line
438 plots of *sox4a*, *atoh1a* and *dld* show that *sox4a* is expressed before *atoh1a* and that
439 *dld* is expressed after *atoh1a* is upregulated (Figures 8G, H).

440 Notch signaling needs to be inhibited for hair cell specification genes to be
441 expressed and we therefore wondered if *sox4a* is regulated by Notch signaling. Indeed,
442 the downregulation of Notch signaling by the γ-secretase inhibitor LY411575, as
443 evidenced by the loss of *her4.1* and *cdkn1bb* expression (Figures 8I, J) leads to the
444 upregulation of *sox4a* and *atoh1a* (Figures 8K-L).

445 Line plots show temporal gene expression changes of well-known hair cell
446 lineage genes with higher granularity than the heatmap in Figure 8A. Line plots reveal
447 that the hair cell specifying genes *atoh1a* and the cell cycle regulator *gadd45gb.1* are
448 upregulated in central support cells before the branch point (Figures 8M, N, stippled

449 line), continue to increase in the hair cell lineage after the branch point (Figure 8N) but
450 are downregulated in the central support cell lineage (Figure 8M). Within the hair cell
451 lineage *atoh1a* and *gadd45gb.1* are followed by *insm1b*, *rbm24a*, *myo6b* and trailed by
452 *gfi1aa* (Figure 8N). Line plots, the heatmap and feature plots also show that cell
453 proliferation (*pcna*, *stmn1a*) occurs in the hair cell lineage (Figure 8P, *dlb*, *dld*, *dlc*,
454 *hes2.2*) after the branch point and that cells in the central support cell lineage do not
455 proliferate (Figure 8O, Figures S10E-F). The high-resolution characterization of gene
456 expression dynamics in the hair cell lineage serves as a reference for developing
457 protocols to induce hair cells in culture and to improve hair cells induction during
458 mammalian regeneration.
459

460 **Hair cell progenitors likely revert back to a central cell fate**

461 When we plotted the distribution of cells in the hair cell lineage along
462 pseudotime, we observed hair cell progenitors clustering with the central support cell
463 lineage (Figure 8Q, green cells). A more detailed analysis of hair cell progenitors from
464 different time points showed that, whereas most of the 3 and 5h hair cell progenitors
465 are located immediately after the branch point close to the hair cell lineage (Figures 8R,
466 S), 10h hair cell progenitors group mostly with the central support cells (Figure 8T)
467 suggesting that these cells had turned on hair cell genes but then failed to fully
468 differentiate and instead turned on central cell genes. We hypothesize that initially
469 more cells are competent to become hair cells but that the re-expression of Notch
470 lateral inhibition signaling between 3-5h ensures that not all cells turn into hair cells but
471 also into support cells (Figure S6E, Figure 7C; [36]). This interpretation is supported by
472 the finding that only few of the *atoh1a* expressing central support cells later turn on *dld*
473 (Figures 8C-D).
474

475 **Overview of cellular and molecular processes during the regeneration time**
476 **course**

477 To identify genes with similar trajectory-dependent expression dynamics and
478 which may be co-regulated, we clustered these genes into units using Monocle 3

479 (Figure S11, Table S6). We identified eight gene units. To gain an understanding of the
480 processes that characterize different stages of regeneration, we performed Enrichment
481 term analysis on unit genes (Figure S11). Unit 3 is comprised of injury response genes.
482 Units 8, 1, and 6 describe genes that are upregulated in cells before the lineage
483 decision branch point and that are then enriched in the hair cell lineage, such as genes
484 involved in ribosome biogenesis/translation, splicing and oxidative phosphorylation.
485 Unit 2 contains genes of the central support cell lineage involved in sensory organ
486 development and stem cell maintenance, and units 4, 7 and 5 contain hair cell lineage
487 genes with the enrichment terms cell cycle, stereocilium organization, glycolysis and
488 glutathione metabolism. Figure 9 synthesizes the dynamic changes of cellular and
489 molecular processes that occur during the three modules of the hair cell regeneration
490 process.
491

492 **Discussion**

493 Inner ear hair cell and lateral line sensory organ development share key
494 regulatory signaling pathways. Yet, unlike fish, mammalian hair cells do not regenerate
495 once damaged. The remarkable speed (3- 5h) at which zebrafish regenerate lateral line
496 hair cells after injury allowed us to characterize the gene expression dynamics of a
497 regenerating vertebrate sensory organ at unprecedented resolution. Our results provide
498 a blueprint of a gene regulatory network that enables support cells to re-enter the cell
499 cycle and replace lost hair cells. Moreover, given that a number of genes/pathways
500 involved in the regeneration of other sensory organs such as the retina in different
501 species are also employed during lateral line regeneration, opens up the possibility that
502 knowledge gained in a particular research organism or organ can inform studies in
503 other species or organ systems (Denans et al., 2019; Hoang et al., 2020; Wan and
504 Goldman, 2016).
505

506 **Gene expression changes occur within minutes after cell death**

507 Our closely timed tissue collections demonstrated that drastic transcriptional
508 changes occur within minutes after hair cell death. Recent studies showed that early

509 response genes are required for triggering regeneration (discussed below). Yet, even
510 though regeneration studies in different species increasingly include scRNA-Seq
511 analysis, the majority of these studies collect only few time points and also collect the
512 first sample many hours, or even days after injury. Our data indicate that in order to
513 gain a complete understanding of the transcriptional dynamics underlying regenerative
514 processes and to allow for comparative analyses between species, it is essential to
515 characterize many closely spaced time points, starting within the first hour after injury.
516

517 **The injury/inflammatory response likely triggers regeneration**

518 Genes expressed within minutes after hair cell death are injury or early response
519 genes that are often involved in inflammation (Figure 3 and Figure 6G; (Bahrami and
520 Drablos, 2016; Cho et al., 2004; Landen et al., 2016; Wang et al., 2020)). Inflammation
521 has pro-regenerative effects in several contexts (Eming et al., 2017; Kyritsis et al.,
522 2012; Namdaran et al., 2012; White et al., 2017). However, the timing of inflammation
523 and its resolution by anti-inflammatory processes is crucial. For example,
524 pharmacological suppression of the immune response before retina and CNS injury in
525 zebrafish leads to a diminished regenerative response; however, blocking inflammation
526 after injury speeds up the regeneration process (Kyritsis et al., 2012; White et al., 2017).
527 These findings suggest that the inflammatory response facilitates the onset of the
528 regeneration process but then needs to be shut off for regeneration to proceed.

529 We did not observe a strong pro-inflammatory response, such as robust *tnfa*,
530 *il1b* or *il6* induction after hair cell death. However, *nr4a1*, a target of *il1b*, *tnfa* and *nfkb*
531 is still strongly induced, as are AP-1 transcription factors (Figures 3A, M; (Pei et al.,
532 2005)). Simultaneously, anti-inflammatory glucocorticoid signaling and *nfkb* inhibitors
533 are rapidly activated at 0min (Figure 3). Interestingly, synthetic glucocorticoid agonists
534 modestly enhance lateral line hair cell regeneration by increasing mitotic activity
535 (Namdaran et al., 2012). Thus, it is possible that the short, pro-inflammatory signal
536 observed in our study may be involved in facilitating hair cell regeneration by
537 minimizing the detrimental effects of a long-term pro-inflammatory response (Denans
538 et al., 2019; Landen et al., 2016; Monje et al., 2003). Jak/Stat3 is also induced at 0min.

539 Loss of *stat3* function causes defects in hair cell regeneration/development in zebrafish
540 and mice (Chen et al., 2017; Liang et al., 2012). The IFNG-pathway responds to hair
541 cell loss at 30min (Figure 3O). It acts upstream of Jak/Stat1 and is involved in skeletal
542 muscle regeneration. Yet, the role of the IFNG-pathway in hair cell regeneration
543 remains to be investigated (Cheng et al., 2008; Zaidi, 2019). All of these early response
544 pathways repress or activate each other in a context-dependent fashion that still needs
545 to be characterized during hair cell regeneration (Cho et al., 2004; Xavier et al., 2016).
546 The AP-1 complex is of particular interest because it is not only required for
547 wound healing but also for regeneration in several contexts (Beauchemin et al., 2015;
548 Ishida et al., 2010; Raivich et al., 2004; Wenemoser et al., 2012). The AP-1 transcription
549 factor complex consists of members of DNA binding proteins, such as Jun, Fos, ATF,
550 JDP and Maf (Hess et al., 2004). Recent studies demonstrated that it is essential for
551 triggering an injury and regeneration response by promoting chromatin accessibility
552 (Beisaw et al., 2020). Additionally, AP-1-motif enriched regeneration responsive
553 enhancers are likely a reason why non-mammalian vertebrates are better at
554 regenerating (Wang et al., 2020). Even though mouse AP-1 enhancer elements drive
555 gene expression in response to injury, they are unable to trigger a regenerative
556 response, likely because of enhancer repurposing during evolution. It would therefore
557 be important to test if AP-1 factors are required for hair cell regeneration in fish and if
558 they are, compare the ability of the fish and mouse AP-1 motif containing enhancers to
559 not only induce an injury- but also a regeneration response. Interestingly, noise
560 induced hair cell damage in the rat cochlea leads to upregulation of the early response
561 genes Egr1, Nr4a1(Nur77) and Btg2, but regeneration is not triggered supporting the
562 notion of enhancer repurposing in mammals (Cho et al., 2004).
563
564 **Regeneration specific genes are active between 30min and 1h**
565 Genes and pathways such as the retinoic acid pathway, which are enriched
566 between 30min and 1h, are relatively regeneration specific, as they are not, or only
567 lowly expressed during homeostasis. They show surprisingly short-lived activation and
568 are again downregulated between 3- 5h. Many of these genes have been implicated in

regeneration, such as *il11* that stimulates progenitor cells in axolotl tail regeneration, Jak/Stat3 and Nr4a1 target *relaxin3a (rln3a)* that is required for zebrafish heart regeneration (Figure 4G, (Fang et al., 2013; Tsujioka et al., 2017; You et al., 2018)). Likewise, the RNA binding protein Lin28 supports mouse axon regeneration, coordinates hair cell progenitor proliferation and differentiation and zebrafish hair cell regeneration (Doetzlhofer and Avraham, 2017; Wang et al., 2018; Ye et al., 2020). Lin28a also leads to enhanced tissue repair by metabolic reprogramming and increased glycolysis and oxidative phosphorylation in mice (Shyh-Chang et al., 2013). It is possible that these genes possess enhancers with AP-1 binding motifs and may represent the switch from a wound healing to a regenerative response, a hypothesis that can be readily tested in future work.

Progenitor/stem cell maintenance/placodal genes are immediately downregulated

During the first 1h of hair cell regeneration more genes are downregulated than upregulated, which could represent a reprogramming step. A number of these genes, such as Notch/Fgf pathway members, *sox*, *six/eya, gata, dlx* and the *antioxidant enzyme glutathione peroxidase 1a* (*gpx1a)* are also expressed in the lateral line placode during development, and their homologs are involved in the development of hair cells in the mammalian inner ear (Figure 2, Figure S3A, (Basch et al., 2016; Kolla et al., 2020; Roccio et al., 2018)). Sox2/3, Six/Eya, Klf, Gata and Dlx transcription factors play multiple roles, such as stem cell maintenance, induction of pluripotency and lineage determination. *gpx1a* has been implicated in ES cell self-renewal (Wang et al., 2014). Likewise, we and others have previously shown that Notch and Fgf pathway downregulation is essential for support cell proliferation and that their re-expression at the end of the regeneration process is required for support cell maintenance (Lush et al., 2019; Ma et al., 2008; Romero-Carvajal et al., 2015). We propose that the downregulated genes are candidates that when temporarily inhibited might improve mammalian support cell reprogramming and hair cell regeneration (Iyer and Groves, 2021).

599

600 **Hair cell specification is triggered in the majority of 3- 5h central support cells but**
601 **only a subset differentiates into hair cells**

602 Between 3- 5h the majority of central support cells upregulate the hair cell
603 specifier *atoh1a* (Figures 5I, 8C, 8F) but then only a subset also activate *dld* and enter
604 the hair cell lineage (Figures 5I, 8D). The other cells maintain *atoh1a* expression for a
605 few hours but simultaneously upregulate central support cell genes and enter the
606 support cell lineage (Figures 8C, D). This finding is in line with what has been observed
607 in Drosophila photoreceptor and zebrafish otic development where Atoh is first broadly
608 expressed and acts as a proneural gene, but subsequently only a subset of the cells
609 acquire a sensory fate (Cai and Groves, 2015). Unexpectedly, even a few *dld*
610 expressing cells appear to revert back to the central support cell lineage (Figure 8D).
611 Figure 8S-T show 5 and 10h hair cell lineage cells that align with central cells along
612 pseudotime. These findings are consistent with recent reports that progenitors of
613 different neural crest cell lineages initially express markers of both lineages and that
614 lineage decisions arise over time (Soldatov et al., 2019). During hair cell development,
615 the re-activation of Notch signaling at 3h correlates with the lineage bifurcation
616 discovered in our pseudotime analysis (Figure 7C). We propose that the re-activation of
617 Notch signaling in the central support cell lineage between 3- 5h may be responsible
618 for ensuring that not all cells enter the hair cell lineage but that the majority of cells
619 returns to a central support cell fate. This interpretation is supported by ours and our
620 colleagues' experimental data that prolonged Notch inhibition causes all cells to adopt
621 a hair cell fate (Ma et al., 2008; Romero-Carvajal et al., 2015).

622

623 **Reactivation of Notch and Fgf signaling inhibits the cell cycle in the central**
624 **support cell lineage**

625 Interestingly, cell proliferation only occurs in the hair cell lineage and not in the
626 central support cell lineage (Figures 8O, P, Figures S10E- F), which corelates with the
627 re-activation of Notch and Fgf signaling in central support cells (Figure 7A). We
628 previously showed that Notch signaling, and to a smaller degree Fgf signaling, inhibit

629 proliferation via the inhibition of Wnt signaling during homeostasis (Lush et al., 2019;
630 Romero-Carvajal et al., 2015). Thus, Notch does not only regulate lineage decisions but
631 also inhibits proliferation and maintains cells in a progenitor state. The antiproliferative
632 effect of Notch signaling is conserved in neural stem cells and the retina (Llorens-
633 Bobadilla et al., 2015; Shin et al., 2015; Wan and Goldman, 2016). Likewise, Fgf
634 signaling inhibits proliferation in the zebrafish retina (Wan and Goldman, 2017).
635 Therefore, important unanswered questions are: what factors lead to the re-activation
636 of Notch and Fgf signaling between 3-5h in the central support cell lineage? And what
637 signals positively drive proliferation in hair cell progenitors upstream of Wnt signaling?
638 (Jacques et al., 2013; Jacques et al., 2012; Romero-Carvajal et al., 2015; Shi et al.,
639 2012; Wang et al., 2015).
640 Amplifying cells in the poles that do not directly give rise to hair cells also
641 proliferate in a Wnt-dependent manner (Figures 1D, 5K heatmap; (Romero-Carvajal et
642 al., 2015)) but it remains to be determined how their proliferation is inhibited during
643 homeostasis, as Notch signaling is not active in the poles (Romero-Carvajal et al.,
644 2015).
645
646 **Ribosome biogenesis and translation significantly increase between 3-5h**
647 Concomitant with hair cell specification, the largest number of transcriptional
648 changes occur at the 3h time point. Ribosome biogenesis and translation (e.g., *npm1a,*
649 *nop56, nop58, RPL* and *RPS genes*) and splicing are activated particularly in the hair
650 cell progenitors (Figures 5A, F-H, O, Figures S6A, B; (Lush et al., 2019)). An increase in
651 ribosome biogenesis has also been observed in immature cardiomyocytes during heart
652 regeneration in newborn mice (Cui et al., 2020). Similarly, ribosome heterogeneity is
653 characteristic for stem cells and the role of regulated ribosome biogenesis during
654 regeneration needs to be interrogated (Gabut et al., 2020; Li and Wang, 2020).
655
656
657

658 **Regeneration recapitulates later stages of hair cell development, but the trigger is**
659 **regeneration specific**
660 Many of the genes and pathways that we identified downstream of *atoh1a* in the
661 hair cell lineage are involved in hair cell development in the mouse, chick and zebrafish
662 implying that the hair cell specification and differentiation process is conserved
663 between development and regeneration. The difference between regeneration and
664 development is that regeneration is likely triggered by an injury/inflammatory response
665 which fails to occur in mammals (Wang et al., 2020). Future studies need to focus on
666 the injury/inflammatory response and downstream targets, to determine why these
667 targets fail to be activated in mammals. Along this line, a gene expression atlas of
668 mammalian inner ear sensory epithelia after damage is needed to identify the block in
669 gene regulation that prevents mammals from regenerating.
670
671 **Similarities with zebrafish cardiac regeneration**
672 Even though we have not yet performed a systematic comparison, we observed
673 that many of the differentially expressed genes that we identified in the regenerating
674 zebrafish lateral line have also been described in other regenerating organs, such as
675 the retina, heart and fin (also (Denans et al., 2019)). For example, during zebrafish
676 cardiac regeneration, the Jak1/Stat3 pathway members *jak1*, *jak3*, *Il6st* and *socs3b* are
677 highly induced, as is *rln3a* (Fang et al., 2013). During zebrafish retina regeneration,
678 several of the same growth factors/cytokines are induced, such as *hb-egf*, *insulin* and
679 *il11* (Wan and Goldman, 2016). As in the lateral line, Notch downregulation leads to
680 proliferation in the retina, which is enhanced by lin28a (Elsaeidi et al., 2018; Romero-
681 Carvajal et al., 2015). Other genes involved in progenitor quiescence are *insm1a* and
682 the Tgfβ inhibitor *tgif1a* (Chablais and Jazwinska, 2012; Lenkowski et al., 2013;
683 Ramachandran et al., 2012). Likewise, some lateral line regeneration genes have also
684 been described in fin and heart regeneration, such as *inhba/b* (Dogra et al., 2017;
685 Sehring et al., 2016; Wang et al., 2020). This gene list is not comprehensive but
686 stresses the value of comparing the regeneration programs between different organs
687 and species to identify candidate regeneration genes. A recent comparison of the

transcriptomes of fish, chick and mouse in Mueller glia after retina injury/regeneration revealed the strength of a comparative approach as they identified gene modules that are shared. However, it also uncovered difficulties. For example, TNF, MAPK, NFKB pathways are activated in mouse and chick Mueller glia cells after retinal injury (Hoang et al., 2020). However, these pathways were not identified in the zebrafish retina regeneration data set, as the earliest time point investigated was at 4h after retina injury, which based on our findings, is too late to observe the initial transcriptional responses. Thus, to gain a complete understanding of the transcriptional dynamics underlying regenerative processes and allow the comparison between species, it is essential to characterize many closely spaced time points, starting within the first hour after injury. High spatio-temporal resolution transcriptome studies from different regenerating species and organs are essential to test our hypothesis that the sequence of the three gene expression modules that we described is conserved and only the length of each module differs.

Conclusion

We have generated a high-resolution regeneration scRNA-Seq data set that will serve as a foundation for devising strategies to help induce hair cell regeneration in mammals. The detailed transcriptome analyses reported here, combined with the characterization of three modules uncovered in our study will also serve as a reference to interrogate similarities in the regeneration response across different species/different organs and in response to different injury paradigms. Thus, this data is not only relevant for our understanding of hair cell regeneration but also for regenerative processes in general.

Acknowledgments

We thank the Piotrowski lab members for insightful discussions and Drs. Alejandro Sánchez Alvarado, Nicolas Denans, Mark Lush, and Jeremy Sandler for critical reading of the manuscript. We thank Jillian Blanck, Jungeun Park, Allison Scott, Jeffrey Lange, Julia Peloggia for technical assistance, Drs. Joaquin Navajas Acedo and

Mark Lush for in situ images, and Mark Miller for graphic design. We are also grateful to the Stowers Institute Core Facilities (Aquatics team, Cytometry Core, Imaging Core, Molecular Biology Core) for their technical expertise. We would also like to thank Dr. Ronna Hertzano, Joshua Orvis and Yang Song for developing and uploading our data to gEAR. This work was funded by an NIH (NIDCD) award 1R01DC015488-01A1 and by institutional support from the Stowers Institute for Medical Research to T.P.

Author Contributions

S.B. designed and performed the experiments, analyzed and interpreted the data, and wrote the manuscript; N.T. analyzed and interpreted the data; D.D. analyzed and interpreted the data; Y-Y. T. performed experiments; T.P. designed the experiments, analyzed and interpreted the data, and wrote the manuscript.

Declaration of interests

The authors declare no competing interests.

Figure titles and legends

Figure 1. Spatio-temporal scRNA-Seq analysis during lateral line hair cell regeneration.

(A) 5dpf *Tg(she:H2A-mCherry)* larvae were used for FACS of lateral line cells.

(B - E) Illustration of homeostatic lateral line cell types. (B, D, E) dorsal view and (C) lateral view.

(F) Confocal images of *Tg(myo6b:H2B-mScarlet-I/et20:GFP)* neuromasts during hair cell regeneration. Scale bar: 20μm, arrow indicates two new hair cells.

(G) Integration of scRNA-Seq samples of seven different time points in UMAP latent space.

(H) UMAP of a cluster analysis identifies eight different neuromast cell types.

(I) Feature plots of cell type-specific marker genes.

(J) Heatmap visualizing the top 25 genes in each timepoint during hair cell regeneration. (Differential gene expression analysis of each time point vs. all other time points)

(K - N) UMAPs of subsetted (K) central support cells, (L) A/P cells, (M) D/V cells and (N) hair cell progenitors with bar graphs showing the number of up and down-regulated genes during regeneration (differential gene expression analysis of each time point vs. homeostasis in individual cell type).

Figure 2. Downregulation of placodal genes, Notch and Fgf- signaling 0min after hair cell death.

(A) Heatmap showing selected cell type-specific downregulated genes 0min after neomycin treatment.

(B) Dot plot displaying the average expression of progenitor/stem cell maintenance/placodal genes during hair cell regeneration. The size of the dots represents the proportion of cells expressing the gene.

(C) ISH images representing *gata2b*, *gpx1a*, and *sox2* expression during hair cell regeneration. Bottom two rows: ISH of *sox2* in sibling and *atoh1a* CRISPR mutant during homeostasis and 0min after neomycin treatment.

(D and E) Dot plots showing the average expression of Notch (D) and Fgf (E) pathway members during hair cell regeneration.

(F) Enrichment term analysis of downregulated genes 0min after hair cell death compared to all other time points.

Figure 3. Injury/inflammatory response genes are rapidly upregulated 0min after hair cell death.

779 (A - B) Heatmap of the expression of selected genes upregulated in all support cells at (A) 0min
780 and (B) 0-30min.
781 (C - F) Heatmaps of genes upregulated in different cell types at 0min and 30min after hair cell
782 death.
783 (G and H) ISH images of (G) *fosab* and (H) *nr4a1* in neuromasts at homeostasis, 0min, 30min,
784 and 1h after hair cell death.
785 (I and J) ISH images of (I) *fosab* and (J) *nr4a1* expression in neuromasts of sibling and *atoh1a*
786 CRISPR mutant embryos at homeostasis and 0min after hair cell death.
787 (K) Confocal images of *Tg(she:H2A-mCherry)* neuromast cells during laser ablation in 5dpf
788 sibling and *atoh1a* mutant embryos.
789 (L) ISH images of *nr4a1* expression in laser-ablated and non-ablated neuromasts of sibling and
790 *atoh1a* CRISPR mutant embryos.
791 (M - O) Dot plots displaying the relative expression of (M) AP-1 TF network members, (N)
792 Glucocorticoid receptor signaling and (O) IFN signaling in neuromasts during hair cell
793 regeneration.
794 (P) Gene enrichment term analysis for genes upregulated 0min after hair cell death compared
795 to all other time points.
796
797 **Figure 4. Upregulated genes 30min – 1h after hair cell death.**
798 (A) Heatmap of the average expression of selected upregulated genes in several support cell
799 types and hair cell progenitors at 30min-1h.
800 (B - E) Heatmaps showing the average expression of genes enriched in different cell types at
801 30min- 1h after hair cell death.
802 (F and G) ISH images of genes upregulated at 30min-1hr in all neuromast cells (F) and central
803 support cells (G).
804 (H and I) Dot plots visualizing the average expression of (H) 'regeneration enriched' genes
805 across seven different regeneration time points and (I) eight different neuromast cell types.
806 (J and K) Dot plots of the average expression of RA pathway genes across (J) seven different
807 regeneration time points and (K) eight different neuromast cell types.
808 (L) Gene enrichment term analysis of up- and downregulated genes at 30min and 1h after hair
809 cell death compared to all other time points.
810

Figure 5. Metabolic reprogramming, ribosome biogenesis and hair cell lineage genes are enriched 3-10h after hair cell death.

(A) Heatmap of the average expression of selected genes in several cell types at 3h- 10h after hair cell death.

(B - E) Heatmaps of the average expression of cell type-specific genes upregulated 3h- 10h after hair cell death.

(F) ISH images of *nop58*, *dla*, and *mcm3* in neuromasts during hair cell regeneration.

(G - L) Dot plots displaying the average expression of (G) ribosome biogenesis, (H) spliceosome, (I) hair cell lineage, (J) cell cycle, (K) Wnt signaling, and (L) Notch signaling. The dot size shows the percentage of cells that express the gene.

(M) Heatmap of the average expression of early and late cell cycle genes in eight different neuromast cell types during hair cell regeneration.

(N - P) Gene enrichment term analysis up- and downregulated genes at (N) 3h, (O) 5h, and (P) 10h after hair cell death compared to all other time points.

Figure 6. Pseudotime analysis (injury response + progenitor activation)

(A - C) UMAPs of pseudotime trajectories of subsetted central support cells and hair cell lineage cells. (A) Dark purple shows cells at the beginning of pseudotime and yellow cells are at the end. (B) UMAP with the location of cells from different time points highlighted in different colors. (C) Cluster analysis groups cells with similar transcriptomes into ten different clusters and shows that, after the branch point cells either follow the central support cell (SC) lineage (blue arrow), or they follow the hair cell lineage (HC lineage, green arrow).

(D) Feature plot of *cd44a* that is enriched in cells before the branch point.

(E) Feature plot of *gata2b* that is enriched in the central support cell (SC) lineage.

(F) Feature plot of *rbm24a* that labels the hair cell lineage.

(G) Heatmap displaying markers selectively enriched in the injury response + progenitor activation population, partitioned into clusters.

(H - J) Feature plots of genes expressed in the injury response + progenitor activation central support cell population.

(K and L) Line plots showing the scaled expression of *fosab*, *irg1l*, and *lima1a* along the pseudotime trajectory in the (K) central support cell (SC) lineage and (L) hair cell lineage (HC). Individual cells are represented by color-coded tics on the x-axis.

845 **Figure 7. Pseudotime analysis (central support cell lineage after the branch point).**
846 (A) Heatmap of the average expression of genes that are selectively enriched in the central
847 support cell lineage, partitioned by louvain clusters.
848 (B) Feature plot of *sox3* and list of other genes expressed in these cells.
849 (C) Feature plot of *hey1* and list of Notch pathway members that are also expressed in these
850 cells.
851 (D) Line plots of the scaled expression of *sox3*, *prox1a*, and *hey1* along the pseudotime
852 trajectory in cells of the central support cell lineage and hair cell lineage cells (HC). Individual
853 cells are represented by color-coded tics on the x-axis.
854
855 **Figure 8. Pseudotime analysis (hair cell (HC) lineage after the branch point)**
856 (A) Heatmap of the average expression of genes that are selectively enriched in HC lineage
857 cells, partitioned by louvain clusters.
858 (B) Feature plot of *sox4a.*
859 (C) Feature plot of *atoh1a.*
860 (D) Feature plot of *dld.*
861 (E) Fluorescent ISH (HCR) images of *sox4a* and *atoh1a* with DAPI in homeostasis, 1h and 3h
862 after hair cell death. Scale bar: 20μm.
863 (G and H) Line plots of *sox4a*, *atoh1a*, and *dld* scaled expression along the pseudotime
864 trajectory in the (G) central support cell lineage and (H) HC lineage. Individual cells are
865 represented by color-coded tics on the x-axis.
866 (I - L) ISH images of *her4.1*, *cdkn1bb*, *sox4a*, and *atoh1a* in 5dpf DMSO- or LY411575-treated
867 (to knock down Notch signaling) neuromasts. Larvae were treated for 6h before fixation.
868 (M and N) Line plots of the scaled expression of *atoh1a*, *insm1b*, *myo6b*, *gadd45gb.*1, *rbm24a*,
869 and *gfi1aa* along the pseudotime trajectory in the (M) the central support cell lineage and (N)
870 HC lineage. Individual cells are represented by color-coded tics on the x-axis.
871 (O and P) Line plots of *dlb*, *dld*, *dlc*, *hes2.2*, *pcna*, and *stmn1a* scaled expression along the
872 pseudotime trajectory in the (O) central support cell lineage and (P) HC lineage.
873 (Q) UMAP highlighting the distribution of HC populations comprising of HC prog, young HC
874 and mature HCs.
875 (R - T) UMAP showing the distribution of 3h, 5h, and 10h HC progenitor populations,
876 respectively.
877 **Figure 9. Overview of the molecular processes occurring during hair cell regeneration.**

878 # STAR Methods

879

880 ## RESOURCE AVAILABILITY

881 ### Lead contact

882 Further information and requests for resources and reagents should be directed to and
883 will be fulfilled by the Lead Contact, Tatjana Piotrowski (pio@stowers.org).

884

885 ### Data and code availability

886 Raw files such as BAM files and count matrices outputted by the CellRanger pipeline
887 have been deposited in the Gene Expression Omnibus database,
888 www.ncbi.nlm.nih.gov/geo (accession no. GEO will be submitted). Source code used
889 to build our shiny applications are uploaded to the following repository,
890 https://github.com/Piotrowski-Lab/shiny-apps. Supplementary scripts and wrapper
891 functions used to process our seurat and pseudotime objects are available in the
892 following github repositories: (https://github.com/Piotrowski-Lab/SeuratExtensions,
893 https://github.com/Piotrowski-Lab/CellTrajectoryExtensions). All original source data
894 are deposited in the Stowers Institute Original Data Repository and available online at
895 https://www.stowers.org/research/publications/libpb-1636

896

897 ## EXPERIMENTAL MODEL AND SUBJECT DETAILS

898 ### Zebrafish

899 Animal work followed the guidelines of the animal ethics committee (IACUC
900 review board) at the Stowers Institute for Medical Research. The following zebrafish
901 transgenic and mutant lines were used: *Tg(she:H2A-mCherry)*^{psi57Tg} , *Tg(Myo6:H2B-*
902 *mScarlet-I)*^{psi66Tg} (Peloggia et al., 2021), *Et(Krt4:EGFP)*^{sqet4ET}, *Et(Krt4:EGFP)*^{sqet20ET} (Parinov
903 et al., 2004), *atoh1a*^{psi69} (Navajas Acedo et al., 2019).

904

905

906

907

908 **METHOD DETAILS**

909 **Sensory hair cell ablation**

910 To ablate hair cells, 5dpf embryos were treated with 150~300μM neomycin
911 (Sigma-Aldrich, St Louis, MO, USA) for 30min at 28 °C. Following, embryos were
912 washed with 0.5x E2 medium (7.5 mM NaCl, 0.25 mM KCl, 0.5 mM MgSO4, 75 mM
913 KH2PO4, 25 mM Na2HPO4, 0.5 mM CaCl2, 0.5 mg/L NaHCO3, pH = 7.4) and
914 incubated at 28 °C until further experimental needed.

915

916 ***scRNA-Seq***

917 **Embryo dissociation and FACS**

918 5dpf larvae were anesthetized with tricaine for ~1 min until they stopped moving
919 (1:20 dilution of 4g/L tricaine in 0.5x E2 medium). We used ~1000 mCherry-positive
920 and 50 mCherry-negative (for gating control) larvae. To dissociate the larvae, we
921 placed the larvae into four wells (250 larvae each) containing strainers (BD Falcon Cell
922 Strainer (BD Biosciences, San Jose, USA), quickly rinsed the larvae in ice-cold DPBS
923 and added 4.5 ml cold 0.25% trypsin-EDTA (Thermo Fisher Scientific, Waltham, USA).
924 The larvae (250 each) were then transferred to one 15ml polypropylene conical tube
925 (placed on ice) with a disposable transfer pipet. Then, the embryos were dissociated by
926 trituration with a 1 ml pipette tip for 3min ~ 3min 30 sec on ice. Since the neuromasts
927 are superficial organs, we separated dissociated neuromast cells from the larval bodies
928 by filtering the suspension through a Filcons 70 μm cell strainer (BD Biosciences, San
929 Jose, CA, USA) into a 5ml polypropylene round-bottom tube. Subsequently, we
930 centrifuged the cells at 2000 rpm (720 x g) for 7 min at 4°C. To wash off the trypsin-
931 EDTA, we removed it, added ice-cold DPBS and centrifuged the cells at 2000 rpm (720
932 x g) for 7 min at 4°C. Resuspended cells in fresh ice-cold DPBS were filtered through a
933 35μm strainer (we only use strainer-cap part from 5ml blue cap strainer tubes (Falcon-
934 Corning, Glendale, AZ, USA) into a falcon round bottom 5ml tube (snap cap tube,
935 Falcon-Corning, Glendale, AZ, USA).

936

937

938 **FACS**

939 To collect viable cells, we stained the resuspended cells with Draq5 and DAPI
940 (Final concentration 25 μM DRAQ5 and 2 μg/ml DAPI). Following incubation for 5 min
941 on ice, stained cells were sorted with BD influx cell sorter (BD Biosciences, San Jose,
942 CA, USA) using a 100 μm nozzle at 20 psi and 1X DPBS (Sigma-Aldrich, St Louis,
943 USA). Laser lines used are 355 nm, 488 nm, and 647 nm. DAPI, GFP, and DRAQ5 are
944 collected using 460/50 nm, 528/28 nm, and 720/40 nm filters, respectively. FSC/SSC
945 size selection gate was constructed by back-gating from high GFP expression.
946 Targeted cells were collected into 90% MeOH (in DPBS) directly.

947

948 **10X Chromium scRNA-seq library construction**

949 Methanol fixed cells were handled using the 10x Genomics suggested process
950 and rehydrated with rehydration buffer (1% BSA and 0.5 U/μl RNase-inhibitor in ice-
951 cold DPBS). The maximum recommended volume of single cell suspension (34 μl) was
952 loaded on a Chromium Single Cell Controller (10x Genomics, Pleasanton, CA).
953 Libraries were made using the Chromium Single Cell 3' Library & Gel Bead Kit v2 (10x
954 Genomics) according to manufacturer's instructions. Following the library preparation,
955 short fragment libraries were tested for quality and quantity using an Agilent 2100
956 Bioanalyzer and Invitrogen Qubit Fluorometer. The libraries were sequenced to
957 produce a depth of ~160-330M reads each on the Illumina HiSeq 2500 instrument
958 (Illumina, San Diego, CA, USA) using Rapid SBS v2 chemistry with the following
959 paired-end read lengths: 26 bp on the Read1, 8 bp on the I7 Index and 98 bp on the
960 Read2.

961

962 **scRNA-Seq read alignment and quantification**

963 Raw reads were demultiplexed and aligned to version 10 of the zebrafish
964 reference transcriptome (danRer10, Ensembl release 91) following 10X Genomics's
965 CellRanger (v2.1.1) pipeline. Prior to the downstream QC filtering we obtained the
966 following cell numbers: 5,099 (homeostasis), 6,817 (0min), 6,727 (30min), 13,257 (1h),
967 3,314 (3h), 4,004 (5h) and 3,450 (10h) using CellRanger's cell-association algorithm.

968 Post-filtering, the number of cells per sample were 4335 (homeostasis), 2481 (0min),
969 2704 (30min), 2804 (1h), 2301 (3h), 1619 (5h), and 1829 (10h). The mean number of
970 genes per sample were 726 (homeostasis), 653 (0min), 639 (30min), 650 (1h), 906 (3h)
971 826 (5h) and 797 (10h). All raw data for temporal samples including sorted BAM files
972 and count matrices produced by CellRanger has been deposited in Gene Expression
973 Omnibus (GEO) database, www.ncbi.nlm.nih.gov/geo (accession no. GEOx).
974

975 **Pre-processing, quality filtering and batch integration**

976 To distinguish zebrafish repeated gene symbols with unique Ensembl IDs, we
977 modified the count matrices outputted from the CellRanger pipeline using a custom R
978 script (https://github.com/Piotrowski-Lab/SeuratExtensions). Each repeated gene
979 symbol is annotated with an asterisk followed by an incrementing number. A
980 comprehensive gene list with unique repeated symbol annotations can be downloaded
981 from our interactive web application
982 (https://piotrowskilab.shinyapps.io/neuromast_regeneration_scRNAseq_pub_2021/).
983 Low quality cells or cells containing doublets with reads greater than 6000 and less
984 than 300 genes per cell after combining all samples were filtered from the subsequent
985 analysis. Genes present in less than 10 cells were also removed from the dataset.
986 All seven temporal samples were integrated together following the standard
987 integration pipeline outlined by the R package Seurat (v3.2.0, (Butler et al., 2018)).
988 Here, individual temporal samples were normalized independently using default
989 parameters via Seurat::NormalizeData. The log-normalized expression values are then
990 z-scored on the integrated object via Seurat::ScaleData using default parameters after
991 finding anchoring cells between samples.
992

993 **Dimensional reduction, and cell classification**

994 Choosing an optimal number of principal components (PCs) for dimensional
995 reduction was determined by scree plot using Seurat::ElbowPlot. We selected PCs
996 showing the greatest variance explained until each subsequent PC showed little to no
997 change. We specified 50 total number of PCs to compute and selected the first 10 PCs

998 based on the scree plot to build and shared nearest neighbor (SNN) graph using
999 Seurat::RunPCA and Seurat::FindNeighbors, respectively. Seurat::FindClusters was
1000 used with a resolution of 0.4, resulting in 13 clusters. To visualize cells in two-
1001 dimensional latent space, we used UMAP dimensional reduction technique via
1002 Seurat::RunUMAP using the first 10 PCs aforementioned. Classification of cell clusters
1003 of the integrated dataset were annotated by calculating differential marker expression
1004 via Seurat::FindAllMarkers using default parameters. Annotating universal neuromast
1005 cell types preserved throughout regeneration was achieved via a comprehensive
1006 marker list previously generated by (Lush et al., 2019). Skin contaminant populations
1007 were removed from the subsequent analysis.
1008
1009 **DE analysis or primary analysis**
1010 To distinguish differentially expressed marker genes between time points, we
1011 used Seurat::FindMarkers to compare cells in one query time point against all other
1012 cells (Figure 2-5, Table S3). The time point specific differential gene list was
1013 subsequently used in our gene set enrichment analysis. For all differentially expressed
1014 gene tables, we defined our statistical test using Wilcoxon Rank-test with default
1015 filtering parameters. Only genes with a p-value less than 0.05 were retained. The top 25
1016 differential genes in each timepoint illustrate the expression dynamics between time
1017 points (Figure 1J).
1018
1019 **Gene set enrichment analysis**
1020 Enriched terms at each time point were identified via the R package
1021 ClusterProfiler (v3.14.3, (Yu et al., 2012)) and ReactomePA (v1.30.0, (Yu and He, 2015)).
1022 Visualizing enriched terms was achieved via R package enrichplot (v1.6.1,
1023 https://github.com/YuLab-SMU/enrichplot). To explore terms from multiple pathway
1024 databases, we ran ClusterProfiler::gseGO, ClusterProfiler::gseKEGG,
1025 ReactomePA::gsePathway to access terms in the GO, KEGG, and Reactome
1026 databases respectively. To accommodate pathway databases that only read in Entrez
1027 IDs such as KEGG and Reactome, we converted Ensembl IDs from our differential

1028 gene tables to its complementary Entrez IDs using ClusterProfiler::bitr. For each time
1029 point analysis, we passed in a sorted named vector of mapping IDs and corresponding
1030 average log-fold change values to the enrichment functions aforementioned. We
1031 filtered and integrated meaningful terms, shown in Figure S3B, from the three pathway
1032 databases into a custom terms database via clusterProfiler::GSEA and returned a
1033 gseResult object. Here, we specified the minimal size of each gene set as 2, the
1034 maximum size of genes annotated for testing as 800 and 10,000 permutations. From
1035 the terms summary of each time point analysis, we labelled activated or suppressed
1036 terms by filtering positive and negative normalized enrichment scores (NES)
1037 respectively. All terms summaries from each time point analysis were then
1038 concatenated into a single dataframe to build the dotplot in Figure S3B (Table S3).
1039

1040 **Pseudotime Analysis**

1041 The pseudotime analysis was processed using R package monocle3 v0.2.1(Cui
1042 et al., 2020; Qiu et al., 2017; Trapnell et al., 2014). From our integrated Seurat object,
1043 we subsetted the following hair cell populations: central cells at 0min through 10hr, hair
1044 cell progenitors at 1hr through 10hr, young hair cells at 3hr through 10hr and mature
1045 hair cells at 3hr through 10hr, totaling 3828 cells. Dimensional reduction was
1046 performed in UMAP latent space using Seurat's standard preprocessing pipeline. We
1047 extracted the subsetted counts matrix and corresponding metadata and converted the
1048 processed Seurat object into a cds object. We coerced the UMAP embeddings
1049 previously generated in Seurat into its corresponding slot in the CDS object. A hallmark
1050 feature in the development of monocle3 is its scalability to partition cells to learn
1051 multiple, disjoint trajectories via partitioned approximate graph abstraction (PAGA).
1052 Since our subsetted cell populations have a common transcriptional ancestor, we set
1053 all possible partitions to a single partition to allow the trajectory path to travel through
1054 the entire UMAP embeddings. Thereafter, we fit a principal graph through the entire
1055 UMAP space via monocle3::learn_graph. Here, we controlled for the amount of
1056 branching paths by pruning trajectories that have a path diameter length less than 15.
1057 Next, cells were ordered along pseudotime via monocle3::order_cells, in which we

specified the root of origin at the 0min central cell population. We relabelled cells belonging to the two major branching events as the Central Cell and Hair Cell Lineage via monocle3::choose_graph_segments, where we selected the start and end node pertaining to each lineage path. Cells that are shared between the two lineages prior to the branching point were relabelled as the Injury Response + Progenitor Activation Lineage. To retrieve the exact pseudotime value and UMAP embeddings of the branching point, we built a custom wrapper function, CellTrajectoryExtension::get_branching_point, found in our github repository (https://github.com/Piotrowski-Lab/CellTrajectoryExtensions). In brief, we built a dataframe that includes every node label with its corresponding UMAP embeddings and subsetted for branching nodes using monocle3::branch_nodes. We then identify the approximate cell barcode and corresponding pseudotime value pertaining to the branching node's embeddings.

To identify correlated gene expression along the trajectory, we utilized a spatial autocorrelation test statistic implemented in monocle3::graph_test, which returns a Moran's I value for each gene. To retain all positive, statistically significant autocorrelation values from monocle3::graph_test, we subsetted gene entries with Moran's I greater than or equal to 0.10 and q-value less than 0.05. We then passed in our filtered genes from the graph_test output into monocle3::find_gene_modules to cluster genes into meaningful modules (called units in the text) using Louvain clustering. Here, we parameterized our resolution at 0.0005 and used the first 3 PCs to cluster our genes, resulting in 8 units as shown in Figure S11 To illustrate dynamic expression of genes in each unit, we calculated the z-scored expression of each gene in its corresponding module and averaged the expression of the cells along pseudotime. We then fit a smoothing line connecting the relationship between average expression of genes in each unit and pseudotime using a locally weighted smoothing method (LOESS). We set our degree of smoothing to 20% using the span argument.

1088 **Interactive web application and data repository**

1089 To encourage fast and dynamic visualization of our scRNA-seq data, we built an
1090 interactive web-based graphical user interface (GUI) via R base Shiny
1091 (https://piotrowskilab.shinyapps.io/neuromast_regeneration_scRNAseq_pub_2021/).
1092 The datasets imported in the shiny app includes the integrated neuromast regeneration
1093 and the pseudotime analysis. Features include visualizing user inputted gene
1094 expression via featureplots, dotplots, heatmaps, pseudotime line plots and
1095 comparative differential analysis. Instructions are provided on the homepage of the
1096 web app. In addition, our integrated regeneration data is uploaded to the Gene
1097 Expression Analysis Resource (gEAR) website (https://umgear.org/p?l=e0d00950)(Orvis
1098 et al., 2021).

1099

1100 **Confocal Imaging and laser ablation**

1101 For confocal imaging, zebrafish embryos were embedded in 1% low-melt
1102 agarose (Promega, Madison, USA), which contains 1x tricaine in 0.5x E2 medium in
1103 glass bottom 35 mm dishes (MatTek, Ashland, USA). Imaging was performed using a
1104 Zeiss LSM 780 confocal microscope with 10x or 40x objectives. All images were
1105 processed using Fiji (Schindelin et al., 2012) software. To ablate specific neuromast
1106 cells, 5dpf of *atoh1a* sibling or mutant embryos *Tg(she:H2A-mCherry)*^{psi57Tg} were
1107 mounted in 1% low-melt agarose with 1x tricaine in 0.5x E2 medium in glass bottom
1108 35 mm dishes. Neuromasts were identified and ablated using an LSM-780 (Zeiss)
1109 confocal microscope. Tissue fluorescence was excited at 561nm through a 40x LD C-
1110 Apochromat objective (Zeiss, NA = 1.1) and collected back through the same objective,
1111 then through a 562-633nm bandpass filter. Photons were detected with a GaAsP
1112 detector running in photon counting mode. Once the tissue of interest was identified,
1113 ablation occurred with a Ti Sapphire 2 photon laser (Coherent) running at 800nm in
1114 mode-locked mode. The laser power at the back aperture of the objective was 6mW.
1115 Ablation occurred over a user selected ROI by point scanning the 2 photon beam
1116 through the ROI a user specified number of times. These settings were adjusted as

1117 needed to achieve ablation. Successful ablation was verified by imaging the tissue in
1118 transmitted light.
1119
1120 **Notch inhibition**
1121 5dpf wild type larvae were treated with 50μM LY411575 (Selleckchem, Houston,
1122 TX, USA) or 1% DMSO (Sigma-Aldrich, St Louis, MO, USA) as a negative control for 6
1123 hours, then fixed overnight in 4% paraformaldehyde at 4°C.
1124
1125 **In Situ Hybridization**
1126 For conventional ISH, anti-sense RNA probes were generated by PCR with
1127 cDNA from mixed stages of zebrafish embryos using T3 promoter-tagged reverse
1128 primer (Table S7), except *gata2b* (Butko et al., 2015), *sox2* (Kudoh et al., 2001), *txn,*
1129 *cdk1nn, her4.1* (Jiang et al., 2014), *dla* (Appel and Eisen, 1998), *atoh1a* (Itoh and
1130 Chitnis, 2001). Go-Taq (Promega, Madison, USA) was used for PCR reaction and PCR
1131 product was purified by NEB gel extraction kit (New England Biolabs, MA, USA).
1132 Following that, In vitro transcription was performed with T3 RNA polymerase (Promega,
1133 Madison, WI, USA) and DIG-labelled kit (Roche, USA) in a PCR machine at 37°C for 4
1134 hrs. After DNase I treatment at 37°C for 30mins, In vitro transcribed RNA was purified
1135 using RNA clean and concentrator kit (Zymo Research, Irvine, CA, USA) in accordance
1136 with the manufacturer's manual. DIG-labelled RNA probe was diluted as 10 ng/μl in
1137 hybridization buffer and stored at -20°C. Colorimetric in situ hybridization was
1138 performed as described previously (Navajas Acedo et al., 2019). Hybridization chain
1139 reaction (HCR) for *sox4a*-B2 and *atoh1a*-B2 (Choi et al., 2018) was carried out following
1140 the manufacturer's manual, except that we incubated in the probe and amplifier for 48h
1141 each. (Molecular Instruments). The amplifier used was B2-546 (Molecular Instruments).
1142 Stained and fixed larvae were stained with DAPI (5μg/ml) for 30 min at room
1143 temperature and washed three times with 5x SSCT and imaged with a confocal
1144 microscope.
1145
1146

Supplementary Table Legends:

Table S1. Markers for the different cell type clusters.

This spreadsheet contains the differentially expressed gene list (cluster markers) of neuromast cell types from the integrated regeneration dataset via Seurat::FindAllMarkers with default parameters. Genes with p-values greater than 0.05 were omitted from the gene list.

Table S2. All genes present in the scRNA-Seq data set.

This spreadsheet contains a list of all genes within the integrated neuromast regeneration scRNA-Seq dataset. Genes present in the expression matrix were extracted and placed within the gene table column named "Gene.name.uniq" along with their corresponding Ensembl ID, ZFIN ID, description, etc.

Table S3. Differential gene expression between time points.

This spreadsheet corresponds to the differential pseudobulk time point expression analysis. For each differential expression analysis, we compared cells labelling a query timepoint against cells in all other time points using the R call function Seurat::FindMarkers followed by a gene set enrichment analysis using the R package ClusterProfiler.

Table S4. Genes represented in figures.

This spreadsheet contains the list of genes used to plot heatmaps and dotplots corresponding to Figures 1-8, S1-S10, and partitioned into individual tabs. Each tab's gene table contains genes symbols, corresponding Ensembl IDs, descriptions, as well as columns of the average scaled (normalized and z-scored) expression value grouped by the cell identities displayed on the x-axis.

Table S5. Markers for clusters in the pseudotime UMAP.

This spreadsheet contains lists of differentially expressed genes partitioned by clusters ordered along the pseudotime trajectory. We grouped clusters based on

where they fall before and after the major branching event. We labelled clusters 3,2,7,6, which aggregate before the branching point as "Injury reponse + progenitor activation". Clusters 4,9,10 with the end terminus leading to 10hr central cells, we labelled as "Central support cell lineage". Clusters 1,5,8 with the end terminus leading to 10hr central cells, we labelled as "HC lineage".

Table S6. Genes belonging to different modules (units).

This spreadsheet contains outputs of genes clustered into modules (units) along the pseudotime trajectory. Gene tables were generated via monocle3::find_gene_modules after subsetting for genes from the spatial autocorrelation analysis (monocle3::graph_test) with a moran_I greater than or equal to 0.10 and q-value less than 0.05.

Table S7. Primers for in situ hybridization probe generation.

Reference

Appel, B., and Eisen, J.S. (1998). Regulation of neuronal specification in the zebrafish spinal cord by Delta function. Development *125*, 371-380.

Bahrami, S., and Drablos, F. (2016). Gene regulation in the immediate-early response process. Adv Biol Regul *62*, 37-49.

Basch, M.L., Brown, R.M., 2nd, Jen, H.I., and Groves, A.K. (2016). Where hearing starts: the development of the mammalian cochlea. J Anat *228*, 233-254.

Beauchemin, M., Smith, A., and Yin, V.P. (2015). Dynamic microRNA-101a and Fosab expression controls zebrafish heart regeneration. Development *142*, 4026-4037.

Behra, M., Bradsher, J., Sougrat, R., Gallardo, V., Allende, M.L., and Burgess, S.M. (2009). Phoenix is required for mechanosensory hair cell regeneration in the zebrafish lateral line. PLoS Genet *5*, e1000455.

Beisaw, A., Kuenne, C., Guenther, S., Dallmann, J., Wu, C.C., Bentsen, M., Looso, M., and Stainier, D.Y.R. (2020). AP-1 Contributes to Chromatin Accessibility to Promote Sarcomere Disassembly and Cardiomyocyte Protrusion During Zebrafish Heart Regeneration. Circ Res *126*, 1760-1778.

Bermingham, N.A., Hassan, B.A., Price, S.D., Vollrath, M.A., Ben-Arie, N., Eatock, R.A., Bellen, H.J., Lysakowski, A., and Zoghbi, H.Y. (1999). Math1: an essential gene for the generation of inner ear hair cells. Science *284*, 1837-1841.

1212 Bucks, S.A., Cox, B.C., Vlosich, B.A., Manning, J.P., Nguyen, T.B., and Stone, J.S.
1213 (2017). Supporting cells remove and replace sensory receptor hair cells in a balance
1214 organ of adult mice. Elife *6*.
1215 Burns, J.C., Cox, B.C., Thiede, B.R., Zuo, J., and Corwin, J.T. (2012). In vivo
1216 proliferative regeneration of balance hair cells in newborn mice. J Neurosci *32*, 6570-
1217 6577.
1218 Burns, J.C., Kelly, M.C., Hoa, M., Morell, R.J., and Kelley, M.W. (2015). Single-cell
1219 RNA-Seq resolves cellular complexity in sensory organs from the neonatal inner ear.
1220 Nat Commun *6*, 8557.
1221 Burns, J.C., and Stone, J.S. (2017). Development and regeneration of vestibular hair
1222 cells in mammals. Semin Cell Dev Biol *65*, 96-105.
1223 Butko, E., Distel, M., Pouget, C., Weijts, B., Kobayashi, I., Ng, K., Mosimann, C.,
1224 Poulain, F.E., McPherson, A., Ni, C.-W.*, et al.* (2015). Gata2b is a restricted early
1225 regulator of hemogenic endothelium in the zebrafish embryo. Development *142*, 1050-
1226 1061.
1227 Butler, A., Hoffman, P., Smibert, P., Papalexi, E., and Satija, R. (2018). Integrating
1228 single-cell transcriptomic data across different conditions, technologies, and species.
1229 Nature Biotechnology *36*, 411-420.
1230 Cai, T., and Groves, A.K. (2015). The Role of Atonal Factors in Mechanosensory Cell
1231 Specification and Function. Mol Neurobiol *52*, 1315-1329.
1232 Chablais, F., and Jazwinska, A. (2012). The regenerative capacity of the zebrafish heart
1233 is dependent on TGFbeta signaling. Development *139*, 1921-1930.
1234 Chen, P., Johnson, J.E., Zoghbi, H.Y., and Segil, N. (2002). The role of Math1 in inner
1235 ear development: Uncoupling the establishment of the sensory primordium from hair
1236 cell fate determination. Development *129*, 2495-2505.
1237 Chen, Q., Quan, Y., Wang, N., Xie, C., Ji, Z., He, H., Chai, R., Li, H., Yin, S., Chin, Y.E.*,*
1238 *et al.* (2017). Inactivation of STAT3 Signaling Impairs Hair Cell Differentiation in the
1239 Developing Mouse Cochlea. Stem Cell Reports *9*, 231-246.
1240 Cheng, M., Nguyen, M.H., Fantuzzi, G., and Koh, T.J. (2008). Endogenous interferon-
1241 gamma is required for efficient skeletal muscle regeneration. Am J Physiol Cell Physiol
1242 *294*, C1183-1191.
1243 Cho, Y., Gong, T.W., Kanicki, A., Altschuler, R.A., and Lomax, M.I. (2004). Noise
1244 overstimulation induces immediate early genes in the rat cochlea. Brain Res Mol Brain
1245 Res *130*, 134-148.
1246 Corwin, J.T., and Cotanche, D.A. (1988). Regeneration of sensory hair cells after
1247 acoustic trauma. Science *240*, 1772-1774.
1248 Corwin, J.T., and Warchol, M.E. (1991). Auditory hair cells: structure, function,
1249 development, and regeneration. Annu Rev Neurosci *14*, 301-333.
1250 Cox, B.C., Chai, R., Lenoir, A., Liu, Z., Zhang, L., Nguyen, D.-H., Chalasani, K.,
1251 Steigelman, K.A., Fang, J., Rubel, E.W.*, et al.* (2014). Spontaneous hair cell
1252 regeneration in the neonatal mouse cochlea in vivo. Development (Cambridge,
1253 England) *141*, 816-829.
1254 Cruz, I.A., Kappedal, R., Mackenzie, S.M., Hailey, D.W., Hoffman, T.L., Schilling, T.F.,
1255 and Raible, D.W. (2015). Robust regeneration of adult zebrafish lateral line hair cells
1256 reflects continued precursor pool maintenance. Dev Biol.

1257 Cui, M., Wang, Z., Chen, K., Shah, A.M., Tan, W., Duan, L., Sanchez-Ortiz, E., Li, H.,
1258 Xu, L., Liu, N.*, et al.* (2020). Dynamic Transcriptional Responses to Injury of
1259 Regenerative and Non-regenerative Cardiomyocytes Revealed by Single-Nucleus RNA
1260 Sequencing. Dev Cell *53*, 102-116 e108.
1261 Denans, N., Baek, S., and Piotrowski, T. (2019). Comparing Sensory Organs to Define
1262 the Path for Hair Cell Regeneration. Annu Rev Cell Dev Biol *35*, 567-589.
1263 Doetzlhofer, A., and Avraham, K.B. (2017). Insights into inner ear-specific gene
1264 regulation: Epigenetics and non-coding RNAs in inner ear development and
1265 regeneration. Semin Cell Dev Biol *65*, 69-79.
1266 Dogra, D., Ahuja, S., Kim, H.T., Rasouli, S.J., Stainier, D.Y.R., and Reischauer, S.
1267 (2017). Opposite effects of Activin type 2 receptor ligands on cardiomyocyte
1268 proliferation during development and repair. Nat Commun *8*, 1902.
1269 Du, X., Li, W., Gao, X., West, M.B., Saltzman, W.M., Cheng, C.J., Stewart, C., Zheng,
1270 J., Cheng, W., and Kopke, R.D. (2013). Regeneration of mammalian cochlear and
1271 vestibular hair cells through Hes1/Hes5 modulation with siRNA. In Hear Res, pp. 91-
1272 110.
1273 Elsaeidi, F., Macpherson, P., Mills, E.A., Jui, J., Flannery, J.G., and Goldman, D. (2018).
1274 Notch Suppression Collaborates with Ascl1 and Lin28 to Unleash a Regenerative
1275 Response in Fish Retina, But Not in Mice. J Neurosci *38*, 2246-2261.
1276 Eming, S.A., Wynn, T.A., and Martin, P. (2017). Inflammation and metabolism in tissue
1277 repair and regeneration. Science *356*, 1026-1030.
1278 Fang, Y., Gupta, V., Karra, R., Holdway, J.E., Kikuchi, K., and Poss, K.D. (2013).
1279 Translational profiling of cardiomyocytes identifies an early Jak1/Stat3 injury response
1280 required for zebrafish heart regeneration. Proc Natl Acad Sci U S A *110*, 13416-13421.
1281 Forge, A., Li, L., Corwin, J.T., and Nevill, G. (1993). Ultrastructural evidence for hair cell
1282 regeneration in the mammalian inner ear. Science *259*, 1616-1619.
1283 Furness, D.N. (2015). Molecular basis of hair cell loss. Cell Tissue Res.
1284 Gabut, M., Bourdelais, F., and Durand, S. (2020). Ribosome and Translational Control
1285 in Stem Cells. Cells *9*.
1286 Gnedeva, K., and Hudspeth, A.J. (2015). SoxC transcription factors are essential for
1287 the development of the inner ear. Proc Natl Acad Sci U S A *112*, 14066-14071.
1288 Graham, V., Khudyakov, J., Ellis, P., and Pevny, L. (2003). SOX2 functions to maintain
1289 neural progenitor identity. Neuron *39*, 749-765.
1290 Gubbels, S.P., Woessner, D.W., Mitchell, J.C., Ricci, A.J., and Brigande, J.V. (2008).
1291 Functional auditory hair cells produced in the mammalian cochlea by in utero gene
1292 transfer. Nature *455*, 537-541.
1293 Hall, C.J., Boyle, R.H., Sun, X., Wicker, S.M., Misa, J.P., Krissansen, G.W., Print, C.G.,
1294 Crosier, K.E., and Crosier, P.S. (2014). Epidermal cells help coordinate leukocyte
1295 migration during inflammation through fatty acid-fuelled matrix metalloproteinase
1296 production. Nat Commun *5*, 3880.
1297 Hernandez, P.P., Olivari, F.A., Sarrazin, A.F., Sandoval, P.C., and Allende, M.L. (2007).
1298 Regeneration in zebrafish lateral line neuromasts: expression of the neural progenitor
1299 cell marker sox2 and proliferation-dependent and-independent mechanisms of hair cell
1300 renewal. Dev Neurobiol *67*, 637-654.

1301 Hess, J., Angel, P., and Schorpp-Kistner, M. (2004). AP-1 subunits: quarrel and
1302 harmony among siblings. J Cell Sci *117*, 5965-5973.
1303 Hoang, T., Wang, J., Boyd, P., Wang, F., Santiago, C., Jiang, L., Yoo, S., Lahne, M.,
1304 Todd, L.J., Jia, M.*, et al.* (2020). Gene regulatory networks controlling vertebrate retinal
1305 regeneration. Science *370*.
1306 Ishida, T., Nakajima, T., Kudo, A., and Kawakami, A. (2010). Phosphorylation of Junb
1307 family proteins by the Jun N-terminal kinase supports tissue regeneration in zebrafish.
1308 Dev Biol *340*, 468-479.
1309 Itoh, M., and Chitnis, A.B. (2001). Expression of proneural and neurogenic genes in the
1310 zebrafish lateral line primordium correlates with selection of hair cell fate in
1311 neuromasts. Mech Dev *102*, 263-266.
1312 Iyer, A.A., and Groves, A.K. (2021). Transcription Factor Reprogramming in the Inner
1313 Ear: Turning on Cell Fate Switches to Regenerate Sensory Hair Cells. Front Cell
1314 Neurosci *15*, 660748.
1315 Jacques, B.E., Montgomery, W.H.t., Uribe, P.M., Yatteau, A., Asuncion, J.D., Resendiz,
1316 G., Matsui, J.I., and Dabdoub, A. (2013). The role of Wnt/beta-catenin signaling in
1317 proliferation and regeneration of the developing basilar papilla and lateral line. Dev
1318 Neurobiol.
1319 Jacques, B.E., Puligilla, C., Weichert, R.M., Ferrer-Vaquer, A., Hadjantonakis, A.-K.,
1320 Kelley, M.W., and Dabdoub, A. (2012). A dual function for canonical Wnt/β-catenin
1321 signaling in the developing mammalian cochlea. Development (Cambridge, England)
1322 *139*, 4395-4404.
1323 Jen, H.I., Hill, M.C., Tao, L., Sheng, K., Cao, W., Zhang, H., Yu, H.V., Llamas, J., Zong,
1324 C., Martin, J.F.*, et al.* (2019). Transcriptomic and epigenetic regulation of hair cell
1325 regeneration in the mouse utricle and its potentiation by Atoh1. Elife *8*.
1326 Jiang, L., Romero-Carvajal, A., Haug, J.S., Seidel, C.W., and Piotrowski, T. (2014).
1327 Gene-expression analysis of hair cell regeneration in the zebrafish lateral line. Proc Natl
1328 Acad Sci U S A *111*, E1383-1392.
1329 Kniss, J.S., Jiang, L., and Piotrowski, T. (2016). Insights into sensory hair cell
1330 regeneration from the zebrafish lateral line. Curr Opin Genet Dev *40*, 32-40.
1331 Kolla, L., Kelly, M.C., Mann, Z.F., Anaya-Rocha, A., Ellis, K., Lemons, A., Palermo, A.T.,
1332 So, K.S., Mays, J.C., Orvis, J.*, et al.* (2020). Characterization of the development of the
1333 mouse cochlear epithelium at the single cell level. Nat Commun *11*, 2389.
1334 Korrapati, S., Roux, I., Glowatzki, E., and Doetzlhofer, A. (2013). Notch signaling limits
1335 supporting cell plasticity in the hair cell-damaged early postnatal murine cochlea. PLoS
1336 One *8*, e73276.
1337 Ku, Y.C., Renaud, N.A., Veile, R.A., Helms, C., Voelker, C.C., Warchol, M.E., and
1338 Lovett, M. (2014). The transcriptome of utricle hair cell regeneration in the avian inner
1339 ear. J Neurosci *34*, 3523-3535.
1340 Kudoh, T., Tsang, M., Hukriede, N.A., Chen, X., Dedekian, M., Clarke, C.J., Kiang, A.,
1341 Schultz, S., Epstein, J.A., Toyama, R.*, et al.* (2001). A gene expression screen in
1342 zebrafish embryogenesis. Genome Res *11*, 1979-1987.
1343 Kyritsis, N., Kizil, C., Zocher, S., Kroehne, V., Kaslin, J., Freudenreich, D., Iltzsche, A.,
1344 and Brand, M. (2012). Acute inflammation initiates the regenerative response in the
1345 adult zebrafish brain. Science *338*, 1353-1356.

1346 Landen, N.X., Li, D., and Stahle, M. (2016). Transition from inflammation to
1347 proliferation: a critical step during wound healing. Cell Mol Life Sci *73*, 3861-3885.
1348 Lee, S., Song, J.J., Beyer, L.A., Swiderski, D.L., Prieskorn, D.M., Acar, M., Jen, H.I.,
1349 Groves, A.K., and Raphael, Y. (2020). Combinatorial Atoh1 and Gfi1 induction
1350 enhances hair cell regeneration in the adult cochlea. Sci Rep *10*, 21397.
1351 Lenkowski, J.R., Qin, Z., Sifuentes, C.J., Thummel, R., Soto, C.M., Moens, C.B., and
1352 Raymond, P.A. (2013). Retinal regeneration in adult zebrafish requires regulation of
1353 TGFbeta signaling. Glia *61*, 1687-1697.
1354 Li, D., and Wang, J. (2020). Ribosome heterogeneity in stem cells and development. J
1355 Cell Biol *219*.
1356 Liang, J., Wang, D., Renaud, G., Wolfsberg, T.G., Wilson, A.F., and Burgess, S.M.
1357 (2012). The stat3/socs3a pathway is a key regulator of hair cell regeneration in
1358 zebrafish. [corrected]. J Neurosci *32*, 10662-10673.
1359 Liberzon, A., Birger, C., Thorvaldsdóttir, H., Ghandi, M., Mesirov, Jill P., and Tamayo,
1360 P. (2015). The Molecular Signatures Database Hallmark Gene Set Collection. Cell Syst
1361 *1*, 417-425.
1362 Llorens-Bobadilla, E., Zhao, S., Baser, A., Saiz-Castro, G., Zwadlo, K., and Martin-
1363 Villalba, A. (2015). Single-Cell Transcriptomics Reveals a Population of Dormant Neural
1364 Stem Cells that Become Activated upon Brain Injury. Cell Stem Cell *17*, 329-340.
1365 López-Schier, H., and Hudspeth, A.J. (2006). A two-step mechanism underlies the
1366 planar polarization of regenerating sensory hair cells. Proceedings of the National
1367 Academy of Sciences of the United States of America *103*, 18615-18620.
1368 Lush, M.E., Diaz, D.C., Koenecke, N., Baek, S., Boldt, H., St Peter, M.K., Gaitan-
1369 Escudero, T., Romero-Carvajal, A., Busch-Nentwich, E.M., Perera, A.G.*, et al.* (2019).
1370 scRNA-Seq reveals distinct stem cell populations that drive hair cell regeneration after
1371 loss of Fgf and Notch signaling. Elife *8*.
1372 Lush, M.E., and Piotrowski, T. (2014). Sensory hair cell regeneration in the zebrafish
1373 lateral line. Dev Dyn *243*, 1187-1202.
1374 Ma, E.Y., and Raible, D.W. (2009). Signaling pathways regulating zebrafish lateral line
1375 development. Curr Biol *19*, R381-386.
1376 Ma, E.Y., Rubel, E.W., and Raible, D.W. (2008). Notch signaling regulates the extent of
1377 hair cell regeneration in the zebrafish lateral line. J Neurosci *28*, 2261-2273.
1378 Mackenzie, S.M., and Raible, D.W. (2012). Proliferative regeneration of zebrafish lateral
1379 line hair cells after different ototoxic insults. PloS one *7*, e47257.
1380 Mathieu, J., and Ruohola-Baker, H. (2017). Metabolic remodeling during the loss and
1381 acquisition of pluripotency. Development *144*, 541-551.
1382 Monje, M.L., Toda, H., and Palmer, T.D. (2003). Inflammatory blockade restores adult
1383 hippocampal neurogenesis. Science *302*, 1760-1765.
1384 Namdaran, P., Reinhart, K.E., Owens, K.N., Raible, D.W., and Rubel, E.W. (2012).
1385 Identification of modulators of hair cell regeneration in the zebrafish lateral line. J
1386 Neurosci *32*, 3516-3528.
1387 Navajas Acedo, J., Voas, M.G., Alexander, R., Woolley, T., Unruh, J.R., Li, H., Moens,
1388 C., and Piotrowski, T. (2019). PCP and Wnt pathway components act in parallel during
1389 zebrafish mechanosensory hair cell orientation. Nat Commun *10*, 3993.

1390 Nicolson, T. (2005). The genetics of hearing and balance in zebrafish. Annu Rev Genet
1391 *39*, 9-22.
1392 Orvis, J., Gottfried, B., Kancherla, J., Adkins, R.S., Song, Y., Dror, A.A., Olley, D., Rose,
1393 K., Chrysostomou, E., Kelly, M.C.*, et al.* (2021). gEAR: Gene Expression Analysis
1394 Resource portal for community-driven, multi-omic data exploration. Nat Methods.
1395 Parinov, S., Kondrichin, I., Korzh, V., and Emelyanov, A. (2004). Tol2 transposon-
1396 mediated enhancer trap to identify developmentally regulated zebrafish genes in vivo.
1397 Dev Dyn *231*, 449-459.
1398 Pei, L., Castrillo, A., Chen, M., Hoffmann, A., and Tontonoz, P. (2005). Induction of
1399 NR4A orphan nuclear receptor expression in macrophages in response to inflammatory
1400 stimuli. J Biol Chem *280*, 29256-29262.
1401 Pei, W., Xu, L., Huang, S.C., Pettie, K., Idol, J., Rissone, A., Jimenez, E., Sinclair, J.W.,
1402 Slevin, C., Varshney, G.K.*, et al.* (2018). Guided genetic screen to identify genes
1403 essential in the regeneration of hair cells and other tissues. NPJ Regen Med *3*, 11.
1404 Peloggia, J., Münch, D., Meneses-Giles, P., Romero-Carvajal, A., Lush, M.E., Lawson,
1405 N.D., McClain, M., Pan, Y.A., and Piotrowski, T. (2021). Adaptive cell invasion
1406 maintains lateral line organ homeostasis in response to environmental changes.
1407 Developmental Cell.
1408 Pinto-Teixeira, F., Viader-Llargues, O., Torres-Mejia, E., Turan, M., Gonzalez-Gualda,
1409 E., Pola-Morell, L., and Lopez-Schier, H. (2015). Inexhaustible hair-cell regeneration in
1410 young and aged zebrafish. Biol Open *4*, 903-909.
1411 Qiu, X., Mao, Q., Tang, Y., Wang, L., Chawla, R., Pliner, H.A., and Trapnell, C. (2017).
1412 Reversed graph embedding resolves complex single-cell trajectories. Nat Methods *14*,
1413 979-982.
1414 Raivich, G., Bohatschek, M., Da Costa, C., Iwata, O., Galiano, M., Hristova, M., Nateri,
1415 A.S., Makwana, M., Riera-Sans, L., Wolfer, D.P.*, et al.* (2004). The AP-1 transcription
1416 factor c-Jun is required for efficient axonal regeneration. Neuron *43*, 57-67.
1417 Ramachandran, R., Zhao, X.F., and Goldman, D. (2012). Insm1a-mediated gene
1418 repression is essential for the formation and differentiation of Muller glia-derived
1419 progenitors in the injured retina. Nat Cell Biol *14*, 1013-1023.
1420 Roccio, M., Perny, M., Ealy, M., Widmer, H.R., Heller, S., and Senn, P. (2018).
1421 Molecular characterization and prospective isolation of human fetal cochlear hair cell
1422 progenitors. Nat Commun *9*, 4027.
1423 Romero-Carvajal, A., Navajas Acedo, J., Jiang, L., Kozlovskaja-Gumbriene, A.,
1424 Alexander, R., Li, H., and Piotrowski, T. (2015). Regeneration of Sensory Hair Cells
1425 Requires Localized Interactions between the Notch and Wnt Pathways. Dev Cell *34*,
1426 267-282.
1427 Ryals, B.M., and Rubel, E.W. (1988). Hair cell regeneration after acoustic trauma in
1428 adult Coturnix quail. Science *240*, 1774-1776.
1429 Sarkar, A., and Hochedlinger, K. (2013). The sox family of transcription factors:
1430 versatile regulators of stem and progenitor cell fate. Cell Stem Cell *12*, 15-30.
1431 Sayyid, Z.N., Wang, T., Chen, L., Jones, S.M., and Cheng, A.G. (2019). Atoh1 Directs
1432 Regeneration and Functional Recovery of the Mature Mouse Vestibular System. Cell
1433 Rep *28*, 312-324 e314.

1434 Scheffer, D.I., Shen, J., Corey, D.P., and Chen, Z.Y. (2015). Gene Expression by Mouse
1435 Inner Ear Hair Cells during Development. J Neurosci *35*, 6366-6380.
1436 Scheibinger, M., Ellwanger, D.C., Corrales, C.E., Stone, J.S., and Heller, S. (2018).
1437 Aminoglycoside Damage and Hair Cell Regeneration in the Chicken Utricle. J Assoc
1438 Res Otolaryngol *19*, 17-29.
1439 Schindelin, J., Arganda-Carreras, I., Frise, E., Kaynig, V., Longair, M., Pietzsch, T.,
1440 Preibisch, S., Rueden, C., Saalfeld, S., Schmid, B.*, et al.* (2012). Fiji: an open-source
1441 platform for biological-image analysis. Nat Methods *9*, 676-682.
1442 Sehring, I.M., Jahn, C., and Weidinger, G. (2016). Zebrafish fin and heart: what's
1443 special about regeneration? Curr Opin Genet Dev *40*, 48-56.
1444 Shi, F., Kempfle, J.S., and Edge, A.S. (2012). Wnt-responsive Lgr5-expressing stem
1445 cells are hair cell progenitors in the cochlea. J Neurosci *32*, 9639-9648.
1446 Shin, J., Berg, D.A., Zhu, Y., Shin, J.Y., Song, J., Bonaguidi, M.A., Enikolopov, G.,
1447 Nauen, D.W., Christian, K.M., Ming, G.L.*, et al.* (2015). Single-Cell RNA-Seq with
1448 Waterfall Reveals Molecular Cascades underlying Adult Neurogenesis. Cell Stem Cell
1449 *17*, 360-372.
1450 Shyh-Chang, N., and Ng, H.H. (2017). The metabolic programming of stem cells.
1451 Genes Dev *31*, 336-346.
1452 Shyh-Chang, N., Zhu, H., Yvanka de Soysa, T., Shinoda, G., Seligson, M.T., Tsanov,
1453 K.M., Nguyen, L., Asara, J.M., Cantley, L.C., and Daley, G.Q. (2013). Lin28 enhances
1454 tissue repair by reprogramming cellular metabolism. Cell *155*, 778-792.
1455 Soldatov, R., Kaucka, M., Kastriti, M.E., Petersen, J., Chontorotzea, T., Englmaier, L.,
1456 Akkuratova, N., Yang, Y., Haring, M., Dyachuk, V.*, et al.* (2019). Spatiotemporal
1457 structure of cell fate decisions in murine neural crest. Science *364*.
1458 Steiner, A.B., Kim, T., Cabot, V., and Hudspeth, A.J. (2014). Dynamic gene expression
1459 by putative hair-cell progenitors during regeneration in the zebrafish lateral line.
1460 Proceedings of the National Academy of Sciences of the United States of America *111*,
1461 E1393-1401.
1462 Thomas, E.D., and Raible, D.W. (2019). Distinct progenitor populations mediate
1463 regeneration in the zebrafish lateral line. Elife *8*.
1464 Trapnell, C., Cacchiarelli, D., Grimsby, J., Pokharel, P., Li, S., Morse, M., Lennon, N.J.,
1465 Livak, K.J., Mikkelsen, T.S., and Rinn, J.L. (2014). The dynamics and regulators of cell
1466 fate decisions are revealed by pseudotemporal ordering of single cells. Nature
1467 Biotechnology *32*, 381-386.
1468 Tsujioka, H., Kunieda, T., Katou, Y., Shirahige, K., Fukazawa, T., and Kubo, T. (2017).
1469 interleukin-11 induces and maintains progenitors of different cell lineages during
1470 Xenopus tadpole tail regeneration. Nat Commun *8*, 495.
1471 Valdivia, L.E., Young, R.M., Hawkins, T.A., Stickney, H.L., Cavodeassi, F., Schwarz, Q.,
1472 Pullin, L.M., Villegas, R., Moro, E., Argenton, F.*, et al.* (2011). Lef1-dependent
1473 Wnt/beta-catenin signalling drives the proliferative engine that maintains tissue
1474 homeostasis during lateral line development. Development *138*, 3931-3941.
1475 Viader-Llargues, O., Lupperger, V., Pola-Morell, L., Marr, C., and Lopez-Schier, H.
1476 (2018). Live cell-lineage tracing and machine learning reveal patterns of organ
1477 regeneration. Elife *7*.

1478 Wagner, E.L., and Shin, J.B. (2019). Mechanisms of Hair Cell Damage and Repair.
1479 Trends Neurosci *42*, 414-424.
1480 Wan, J., and Goldman, D. (2016). Retina regeneration in zebrafish. Curr Opin Genet
1481 Dev *40*, 41-47.
1482 Wan, J., and Goldman, D. (2017). Opposing Actions of Fgf8a on Notch Signaling
1483 Distinguish Two Muller Glial Cell Populations that Contribute to Retina Growth and
1484 Regeneration. Cell Rep *19*, 849-862.
1485 Wan, L., Lovett, M., Warchol, M.E., and Stone, J.S. (2020). Vascular endothelial growth
1486 factor is required for regeneration of auditory hair cells in the avian inner ear. Hear Res
1487 *385*, 107839.
1488 Wang, Q.Y., Liu, Z.S., Wang, J., Wang, H.X., Li, A., Yang, Y., Wang, X.Z., Zhao, Y.Q.,
1489 Han, Q.Y., Cai, H.*, et al.* (2014). Glutathione peroxidase-1 is required for self-renewal of
1490 murine embryonic stem cells. Biochem Biophys Res Commun *448*, 454-460.
1491 Wang, T., Chai, R., Kim, G.S., Pham, N., Jansson, L., Nguyen, D.H., Kuo, B., May, L.A.,
1492 Zuo, J., Cunningham, L.L.*, et al.* (2015). Lgr5+ cells regenerate hair cells via
1493 proliferation and direct transdifferentiation in damaged neonatal mouse utricle. Nat
1494 Commun *6*, 6613.
1495 Wang, W., Hu, C.K., Zeng, A., Alegre, D., Hu, D., Gotting, K., Ortega Granillo, A., Wang,
1496 Y., Robb, S., Schnittker, R.*, et al.* (2020). Changes in regeneration-responsive
1497 enhancers shape regenerative capacities in vertebrates. Science *369*.
1498 Wang, X.W., Li, Q., Liu, C.M., Hall, P.A., Jiang, J.J., Katchis, C.D., Kang, S., Dong,
1499 B.C., Li, S., and Zhou, F.Q. (2018). Lin28 Signaling Supports Mammalian PNS and CNS
1500 Axon Regeneration. Cell Rep *24*, 2540-2552 e2546.
1501 Warchol, M.E., and Corwin, J.T. (1996). Regenerative proliferation in organ cultures of
1502 the avian cochlea: identification of the initial progenitors and determination of the
1503 latency of the proliferative response. J Neurosci *16*, 5466-5477.
1504 Wenemoser, D., Lapan, S.W., Wilkinson, A.W., Bell, G.W., and Reddien, P.W. (2012). A
1505 molecular wound response program associated with regeneration initiation in
1506 planarians. Genes Dev *26*, 988-1002.
1507 White, D.T., Sengupta, S., Saxena, M.T., Xu, Q., Hanes, J., Ding, D., Ji, H., and Mumm,
1508 J.S. (2017). Immunomodulation-accelerated neuronal regeneration following selective
1509 rod photoreceptor cell ablation in the zebrafish retina. Proc Natl Acad Sci U S A *114*,
1510 E3719-E3728.
1511 White, P.M., Doetzlhofer, A., Lee, Y.S., Groves, A.K., and Segil, N. (2006). Mammalian
1512 cochlear supporting cells can divide and trans-differentiate into hair cells. Nature *441*,
1513 984-987.
1514 Whitfield, T.T. (2002). Zebrafish as a model for hearing and deafness. J Neurobiol *53*,
1515 157-171.
1516 Wibowo, I., Pinto-Teixeira, F., Satou, C., Higashijima, S.-i., and López-Schier, H.
1517 (2011). Compartmentalized Notch signaling sustains epithelial mirror symmetry.
1518 Development (Cambridge, England) *138*, 1143-1152.
1519 Wong, A.C., and Ryan, A.F. (2015). Mechanisms of sensorineural cell damage, death
1520 and survival in the cochlea. Front Aging Neurosci *7*, 58.
1521 Woods, C., Montcouquiol, M., and Kelley, M.W. (2004). Math1 regulates development
1522 of the sensory epithelium in the mammalian cochlea. Nat Neurosci *7*, 1310-1318.

1523 Xavier, A.M., Anunciato, A.K., Rosenstock, T.R., and Glezer, I. (2016). Gene Expression
1524 Control by Glucocorticoid Receptors during Innate Immune Responses. Front
1525 Endocrinol (Lausanne) *7*, 31.
1526 Ye, Z., Su, Z., Xie, S., Liu, Y., Wang, Y., Xu, X., Zheng, Y., Zhao, M., and Jiang, L.
1527 (2020). Yap-lin28a axis targets let7-Wnt pathway to restore progenitors for initiating
1528 regeneration. Elife *9*.
1529 You, X., Guo, Z.F., Cheng, F., Yi, B., Yang, F., Liu, X., Zhu, N., Zhao, X., Yan, G., Ma,
1530 X.L.*, et al.* (2018). Transcriptional up-regulation of relaxin-3 by Nur77 attenuates beta-
1531 adrenergic agonist-induced apoptosis in cardiomyocytes. J Biol Chem *293*, 14001-
1532 14011.
1533 Yu, G., and He, Q.-Y. (2015). ReactomePA: an R/Bioconductor package for reactome
1534 pathway analysis and visualization. Mol Biosyst *12*, 477-479.
1535 Yu, G., Wang, L.-G., Han, Y., and He, Q.-Y. (2012). clusterProfiler: an R Package for
1536 Comparing Biological Themes Among Gene Clusters. Omics J Integr Biology *16*, 284-
1537 287.
1538 Zaidi, M.R. (2019). The Interferon-Gamma Paradox in Cancer. J Interferon Cytokine
1539 Res *39*, 30-38.
1540 Zheng, J.L., and Gao, W.Q. (2000). Overexpression of Math1 induces robust
1541 production of extra hair cells in postnatal rat inner ears. Nat Neurosci *3*, 580-586.
1542 Zhu, Y., Scheibinger, M., Ellwanger, D.C., Krey, J.F., Choi, D., Kelly, R.T., Heller, S.,
1543 and Barr-Gillespie, P.G. (2019). Single-cell proteomics reveals changes in expression
1544 during hair-cell development. Elife *8*.
1545

Figure 1

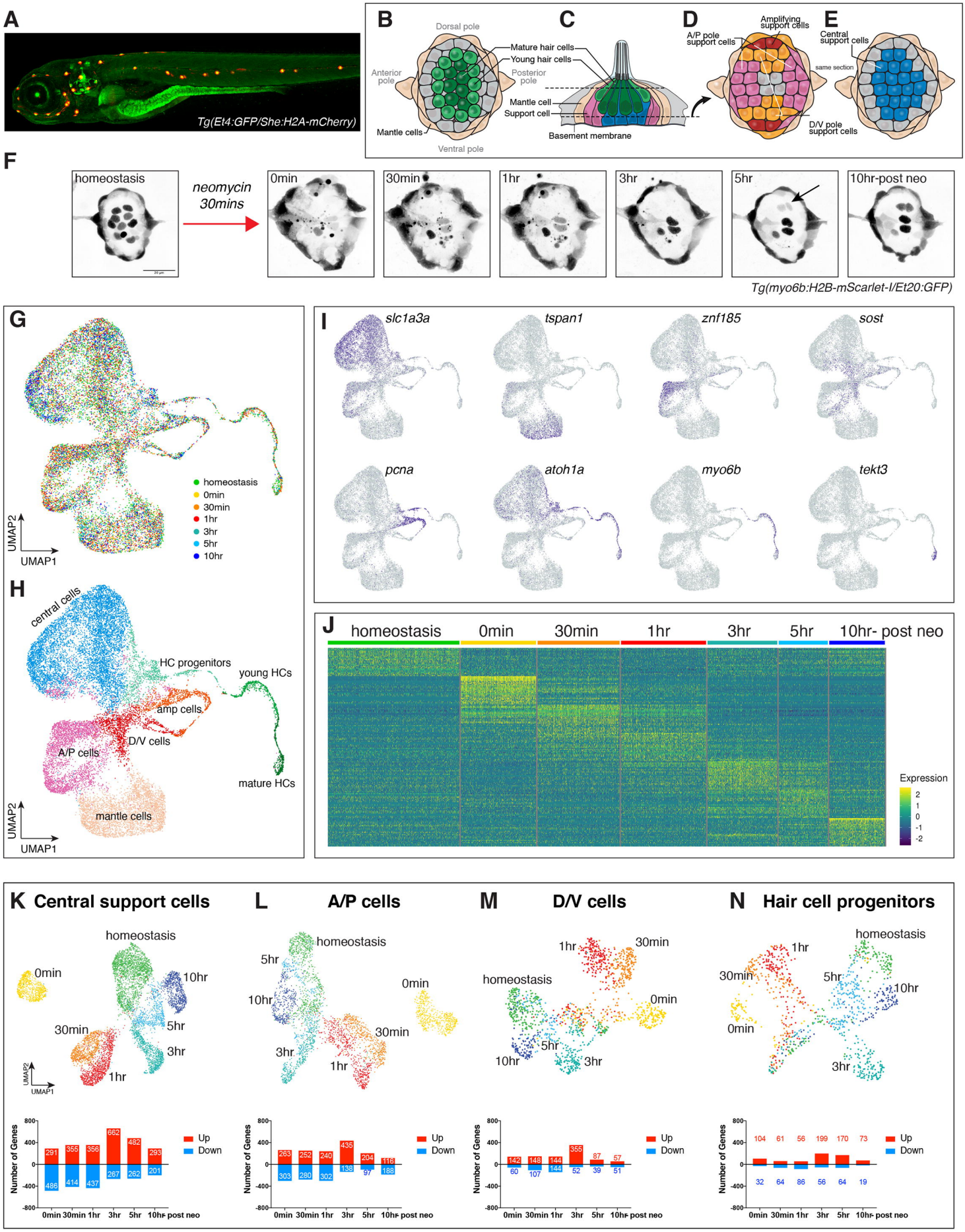
A
Tg(Et4:GFP/She:H2A-mCherry)
B
Dorsal pole
Anterior pole
Posterior pole
Mantle cells
Ventral pole
C
Mature hair cells
Young hair cells
Mantle cell
Support cell
Basement membrane
D
A/P pole support cells
Amplifying support cells
D/V pole support cells
E
Central support cells
same section
F
homeostasis
neomycin 30mins
0min
30min
1hr
3hr
5hr
10hr-post neo
Tg(myo6b:H2B-mScarlet-I/Et20:GFP)
G
homeostasis
0min
30min
1hr
3hr
5hr
10hr
UMAP2
UMAP1
H
central cells
HC progenitors
young HCs
amp cells
D/V cells
A/P cells
mature HCs
mantle cells
UMAP2
UMAP1
I
slc1a3a
tspan1
znf185
sost
pcna
atoh1a
myo6b
tekt3
J
homeostasis
0min
30min
1hr
3hr
5hr
10hr- post neo
Expression
2
1
0
-1
-2
K Central support cells
homeostasis
0min
10hr
30min
5hr
3hr
1hr
UMAP2
UMAP1
L A/P cells
homeostasis
5hr
0min
10hr
30min
3hr
1hr
M D/V cells
1hr
30min
homeostasis
0min
5hr
10hr
3hr
N Hair cell progenitors
homeostasis
1hr
30min
5hr
10hr
0min
3hr
Number of Genes
Up
Down
0min 30min 1hr 3hr 5hr 10hr- post neo
291 355 356 662 482 293
486 414 437 267 262 201
263 252 240 435 204 116
303 280 302 138 97 188
142 148 144 355 87 57
60 107 144 52 39 51
104 61 56 199 170 73
32 64 86 56 64 19

Figure 2 0min downregulated

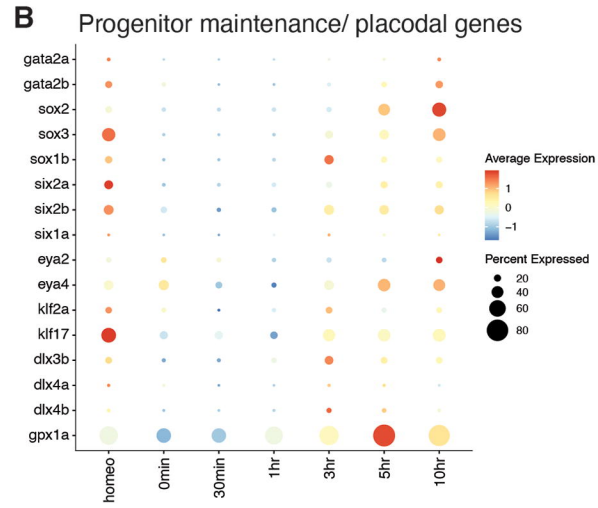

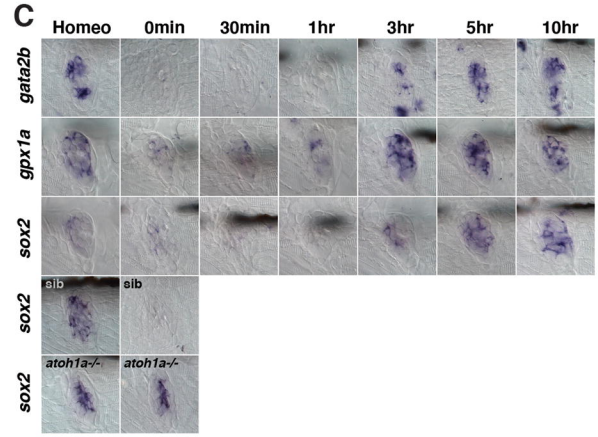

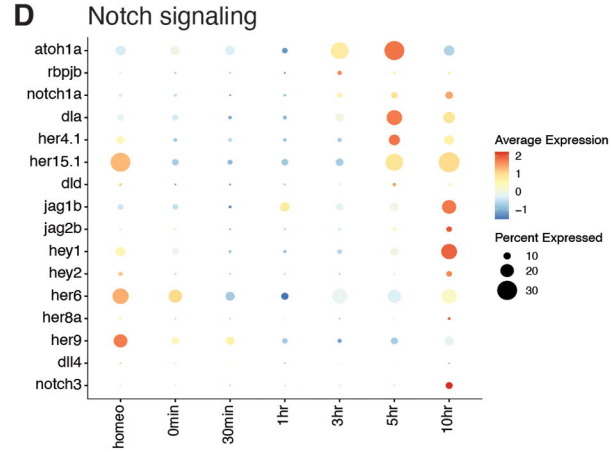

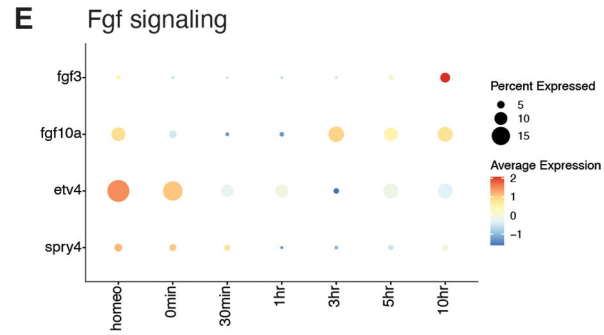

F

Enrichment terms (0min DOWN)	P-value
Notch signaling	5.38E-03
Oxidative phosphorylation	7.25E-04
Ribosome biogenesis	3.51E-04
Spliceosome	2.80E-02

Figure 3 0min upregulated

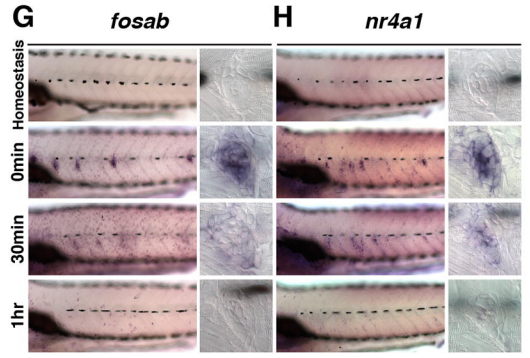

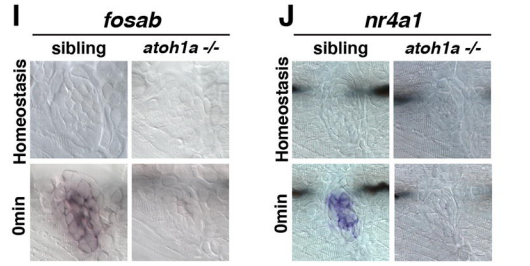

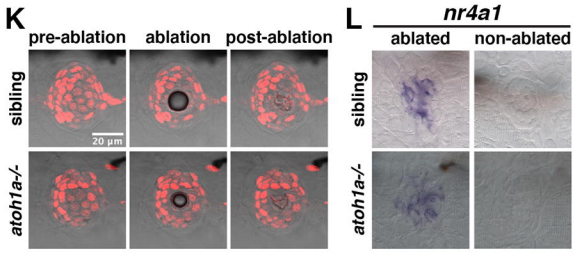

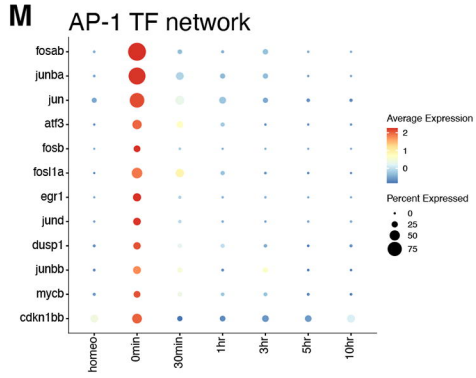

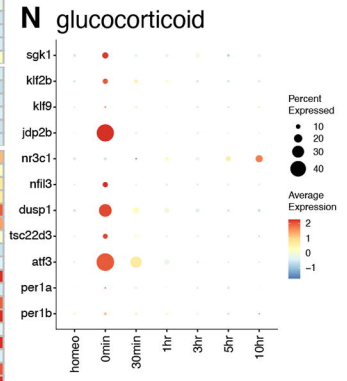

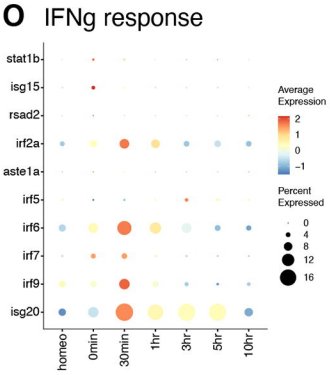

P

Enrichment terms (0min UP)	P-value
Activation of the AP-1 family of TFs	5.58E-04
IFN signaling	5.23E-03
MAPK signaling pathway	8.61E-04
Toll-like receptor signaling	4.09E-03
Cell adhesion molecules	3.35E-02

Figure 4 Upregulated genes 30min -1h after hair cell death

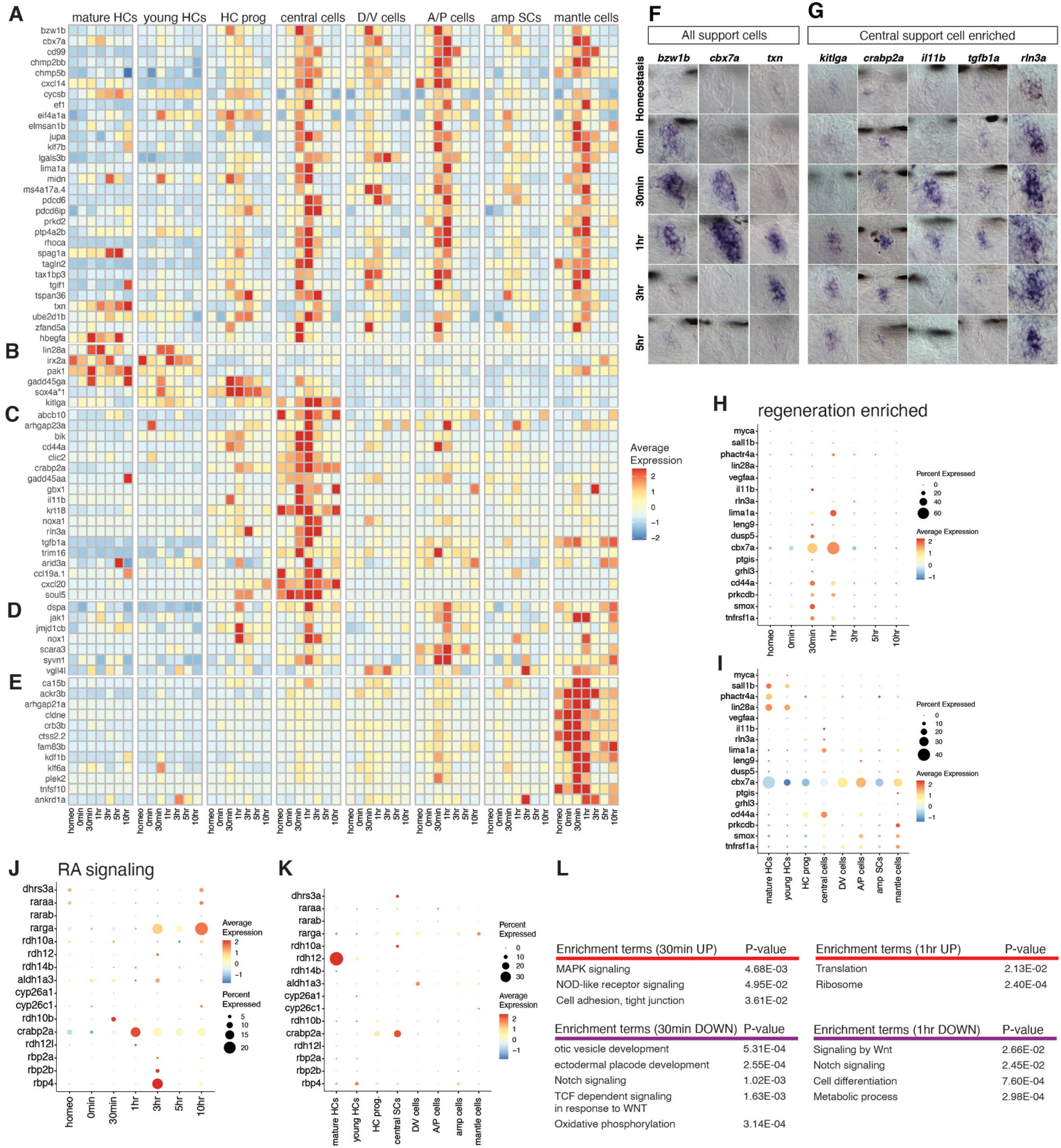

Enrichment terms (30min UP)	P-value
MAPK signaling	4.68E-03
NOD-like receptor signaling	4.95E-02
Cell adhesion, tight junction	3.61E-02

Enrichment terms (1hr UP)	P-value
Translation	2.13E-02
Ribosome	2.40E-04

Enrichment terms (30min DOWN)	P-value
otic vesicle development	5.31E-04
ectodermal placode development	2.55E-04
Notch signaling	1.02E-03
TCF dependent signaling in response to WNT	1.63E-03
Oxidative phosphorylation	3.14E-04

Enrichment terms (1hr DOWN)	P-value
Signaling by Wnt	2.66E-02
Notch signaling	2.45E-02
Cell differentiation	7.60E-04
Metabolic process	2.98E-04

Figure 5 Upregulated genes 3h-10h after hair cell death

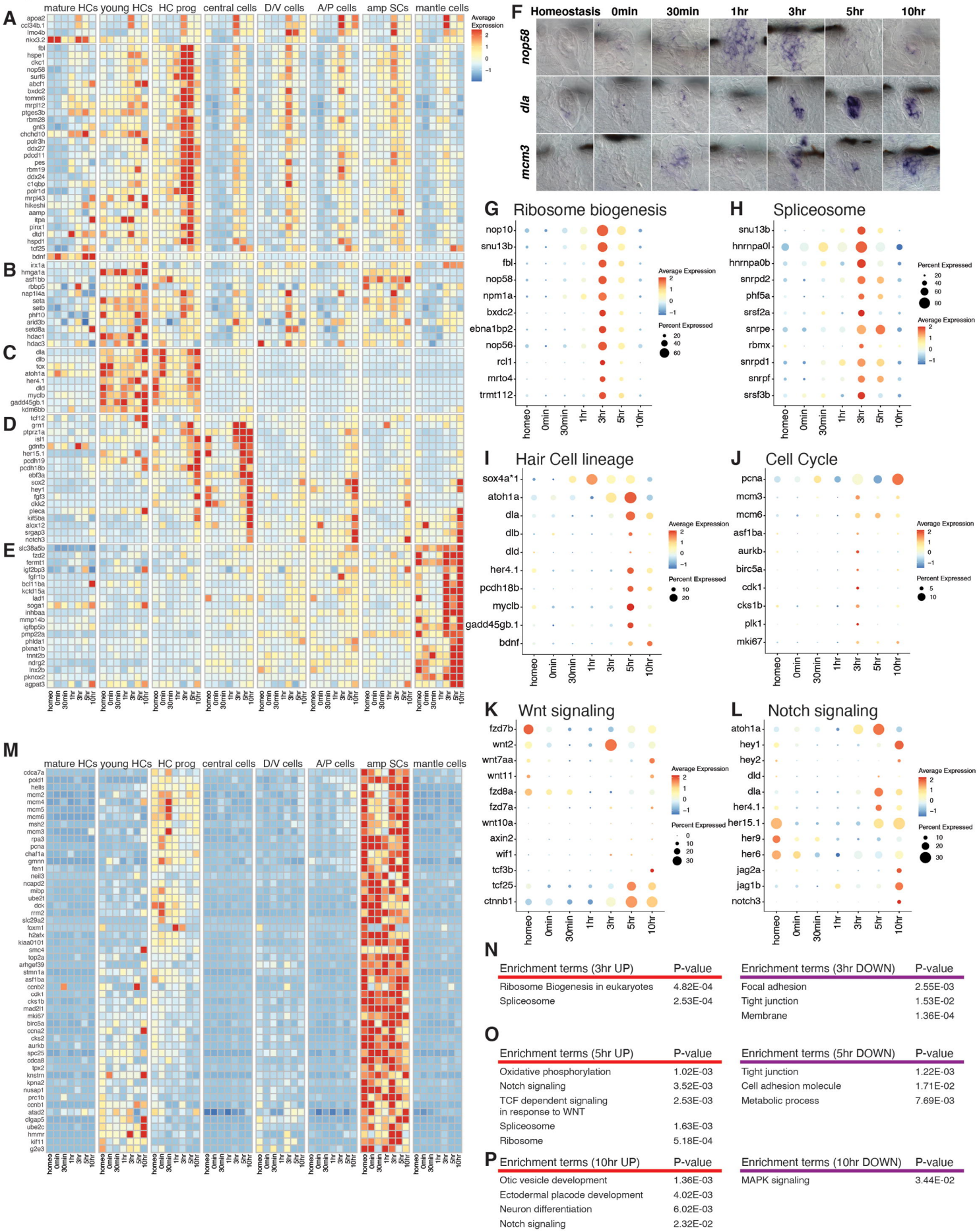

Enrichment terms (3hr UP)	P-value
Ribosome Biogenesis in eukaryotes	4.82E-04
Spliceosome	2.53E-04

Enrichment terms (3hr DOWN)	P-value
Focal adhesion	2.55E-03
Tight junction	1.53E-02
Membrane	1.36E-04

Enrichment terms (5hr UP)	P-value
Oxidative phosphorylation	1.02E-03
Notch signaling	3.52E-03
TCF dependent signaling in response to WNT	2.53E-03
Spliceosome	1.63E-03
Ribosome	5.18E-04

Enrichment terms (5hr DOWN)	P-value
Tight junction	1.22E-03
Cell adhesion molecule	1.71E-02
Metabolic process	7.69E-03

Enrichment terms (10hr UP)	P-value
Otic vesicle development	1.36E-03
Ectodermal placode development	4.02E-03
Neuron differentiation	6.02E-03
Notch signaling	2.32E-02

Enrichment terms (10hr DOWN)	P-value
MAPK signaling	3.44E-02

Figure 6 Pseudotime analysis

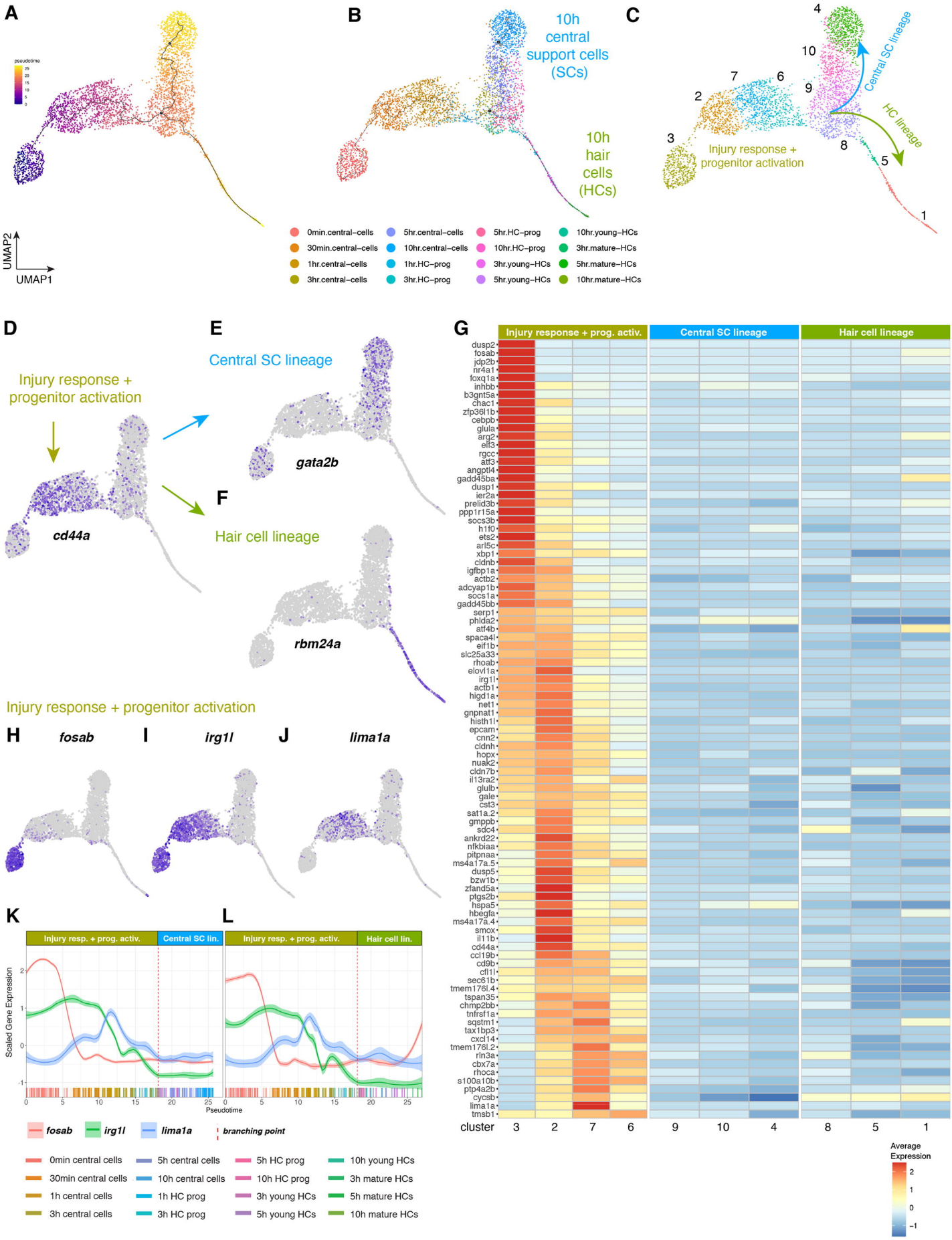

Figure 7 Central support cell lineage

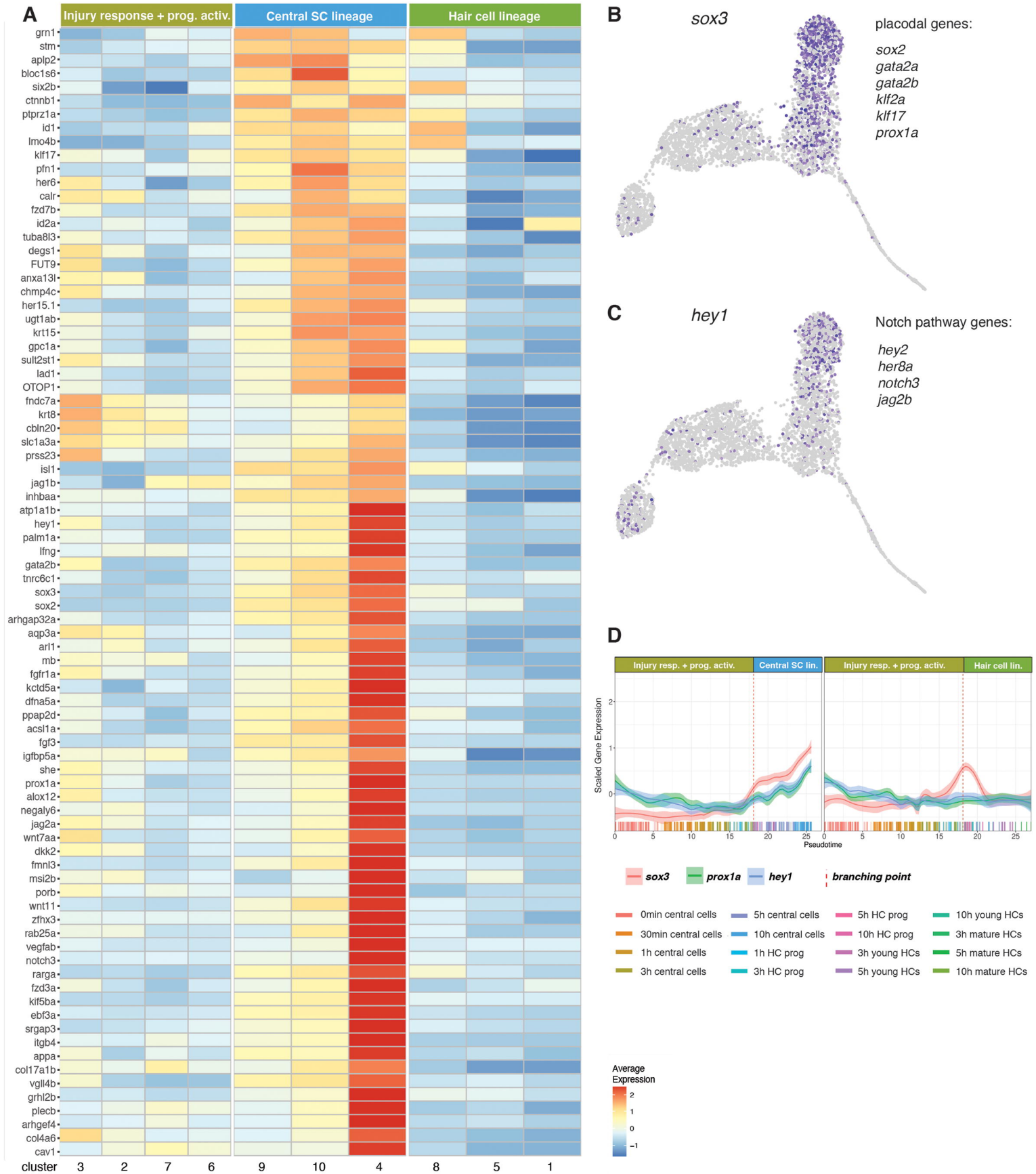

Figure 8 Hair cell lineage

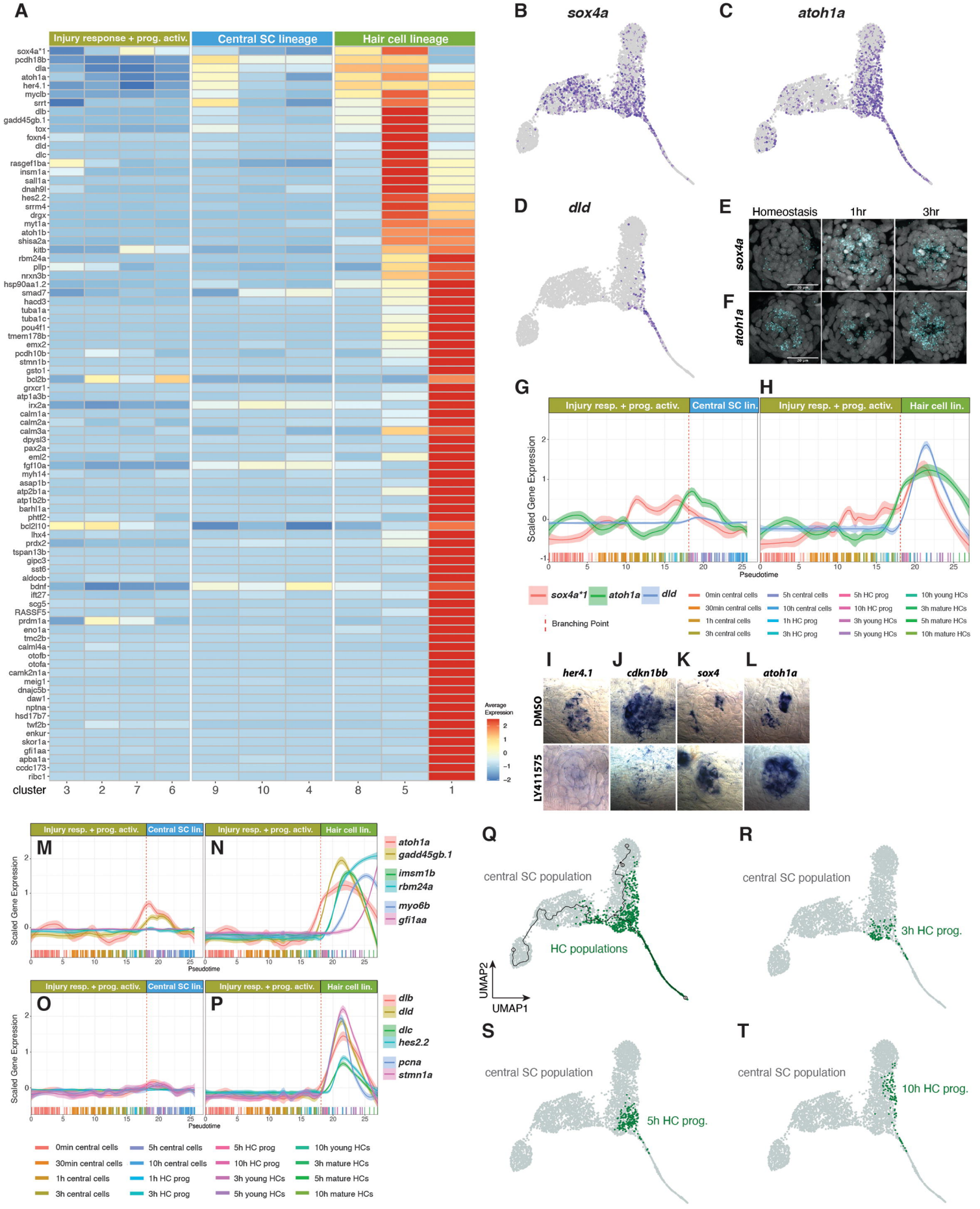

Figure 9

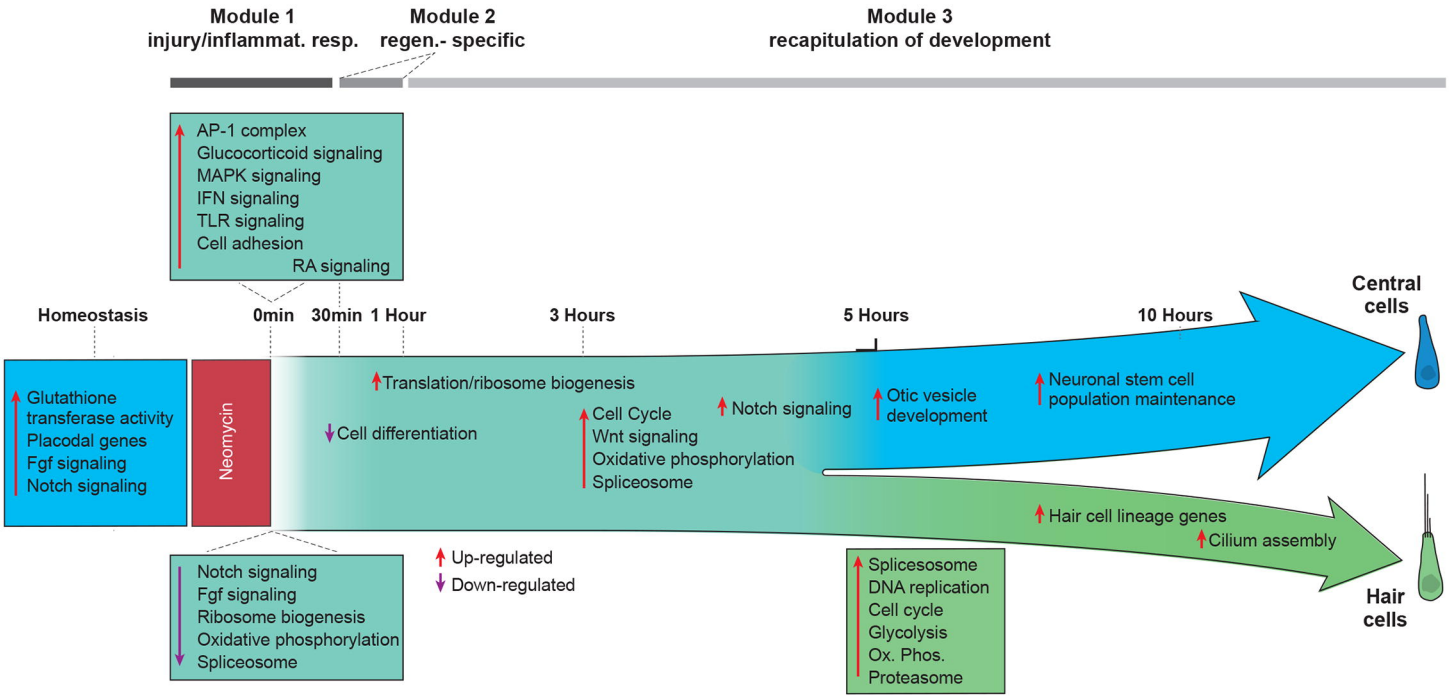
Module 1
injury/inflammat. resp.
Module 2
regen.- specific
Module 3
recapitulation of development
AP-1 complex
Glucocorticoid signaling
MAPK signaling
IFN signaling
TLR signaling
Cell adhesion
RA signaling
Homeostasis
0min
30min
1 Hour
3 Hours
5 Hours
10 Hours
Central cells
Glutathione transferase activity
Placodal genes
Fgf signaling
Notch signaling
Neomycin
Translation/ribosome biogenesis
Cell differentiation
Cell Cycle
Wnt signaling
Oxidative phosphorylation
Spliceosome
Notch signaling
Otic vesicle development
Neuronal stem cell population maintenance
Hair cell lineage genes
Cilium assembly
Hair cells
Notch signaling
Fgf signaling
Ribosome biogenesis
Oxidative phosphorylation
Spliceosome
Up-regulated
Down-regulated
Splicesosome
DNA replication
Cell cycle
Glycolysis
Ox. Phos.
Proteasome